Inorganic Chemistry

Article

pubs.acs.org/IC

Structures, Magnetochemistry, Spectroscopy, Theoretical Study, and Catechol Oxidase Activity of Dinuclear and Dimer-of-Dinuclear Mixed-Valence $Mn^{III}Mn^{II}$ Complexes Derived from a Macrocyclic Ligand

Arpita Jana,[†] Núria Aliaga-Alcalde,[‡] Eliseo Ruiz,*[,§] and Sasankasekhar Mohanta*[,†]

[†]Department of Chemistry, University of Calcutta, 92 A. P. C. Road, Kolkata 700 009, India

[‡]Institució Catalana de Recerca i Estudis Avançats (ICREA), Institut de Ciència de Materials de Barcelona (ICMAB-CSIC) Campus de la UAB, 08193 Bellaterra, Spain

[§]Departament de Química Inorgànica and Institut de Recerca de Química Teòrica i Computacional, Universitat de Barcelona, Diagonal 645, E-08028 Barcelona, Spain

Supporting Information

ABSTRACT: The work in this paper presents syntheses, characterization, magnetic properties (experimental and density functional theoretical), catecholase activity, and electrospray ionization mass spectroscopic (ESI-MS positive) studies of two mixed-valence dinuclear $Mn^{III}Mn^{II}$ complexes, $[Mn^{III}Mn^{II}L(\mu\text{-}O_2CMe)(H_2O)_2](ClO_4)_2\cdot H_2O\cdot MeCN$ (**1**) and $[Mn^{III}Mn^{II}L(\mu\text{-}O_2CPh)(MeOH)(ClO_4)](ClO_4)$ (**2**), and a $Mn^{III}Mn^{II}Mn^{II}Mn^{III}$ complex, $[\{Mn^{III}Mn^{II}L(\mu\text{-}O_2CEt)(EtOH)\}_2(\mu\text{-}O_2CEt)](ClO_4)_3$ (**3**), derived from the Robson-type macrocycle H_2L, which is the [2 + 2] condensation product of 2,6-diformyl-4-methylphenol and 2,2-dimethyl-1,3-diaminopropane. In **1** and **2** and in two $Mn^{III}Mn^{II}$ units in **3**, the two metal centers are bridged by a bis(μ-phenoxo)-μ-carboxylate moiety. The two Mn^{II} centers of the two $Mn^{III}Mn^{II}$ units in **3** are bridged by a propionate moiety, and therefore this compound is a dimer of two dinuclear units. The coordination geometry of the Mn^{III} and Mn^{II} centers are Jahn–Teller distorted octahedral and distorted trigonal prism, respectively. Magnetic studies reveal weak ferro- or antiferromagnetic interactions between the Mn^{III} and Mn^{II} centers in **1** (J = +0.08 cm^{-1}), **2** (J = −0.095 cm^{-1}), and **3** (J_1 = +0.015 cm^{-1}). A weak antiferromagnetic interaction (J_2 = −0.20 cm^{-1}) also exists between the Mn^{II} centers in **3**. DFT methods properly reproduce the nature of the exchange interactions present in such systems. A magneto-structural correlation based on Mn–O bridging distances has been proposed to explain the different sign of the exchange coupling constants. Utilizing 3,5-di-*tert*-butyl catechol (3,5-$DTBCH_2$) as the substrate, catecholase activity of all the three complexes has been checked in MeCN and MeOH, revealing that all three are active catalysts with K_{cat} values lying in the range 7.5–64.7 h^{-1}. Electrospray ionization mass (ESI-MS positive) spectra of the complexes **1**–**3** have been recorded in MeCN solutions, and the positive ions have been well characterized. ESI-MS positive spectrum of complex **1** in presence of 3,5-$DTBCH_2$ has also been recorded, and a positive ion, $[Mn^{III}Mn^{II}L(\mu\text{-}3,5\text{-}DTBC^{2-})]^+$, having most probably a bridging catecholate moiety has been identified.

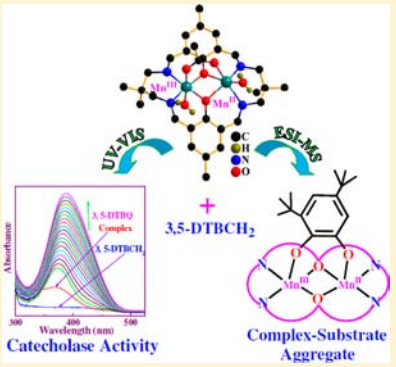

INTRODUCTION

The research area of mixed-valence metal complexes has been a frontier field over a few decades.[1−7] The major foci in this area include the understanding of the role of the ligand environment to affect the extent of electron localization/delocalization resulting in Class I/II/III systems and the possible use of mixed-valence systems in molecular electronics and molecular computing. In this sense, several mixed valence metal complexes are also known to exhibit slow magnetic relaxation.[4,5] It is worth mentioning that the reported single molecule magnets are dominated by mixed-valence manganese clusters.[5] Another key aspect of mixed-valence complexes is related to the presence of such systems in a number of metallo-biomolecules.[6−8] The studies of manganese compounds are in general important due to the presence of the ions in different oxidation states in metallo-biomolecules such as superoxide dismutase,[6c,9a] catalase,[9b,c] photosystem II[8] of green plants, etc.

Catechol oxidase is a copper enzyme having a hydroxo-bridged dicopper(II) center in the active site. This enzyme catalyzes the oxidation of a wide range of *o*-diphenols (catechols) to the corresponding *o*-quinones coupled with $2e/2H^+$ reduction of O_2 to H_2O, in a process known as catecholase activity.[10−15] Extensive biomimetic studies have been carried out taking dicopper(II) complexes, derived from nitrogen-containing dinucleating ligands, as the model com-

Received: April 13, 2013
Published: June 10, 2013

   dx.doi.org/10.1021/ic400916h | Inorg. Chem. 2013, 52, 7732−7746

pounds. While the metallo-enzyme contains hydroxo-bridged dicopper(II), activity has been observed for dicopper(II) systems having hydroxo[10,12] or various other bridging moieties.[10,12a,13] Again, although the active site contains dicopper(II) center, some mononuclear, oligonuclear, and polymeric copper(II) complexes have also been found to show the activity.[10,11,12a] Moreover, mononuclear, dinuclear, and oligonuclear complexes of other metals such as manganese, iron, and cobalt are also known to behave as catalysts,[16−20] indicating the importance of the exploration of catecholase activity by new types of complexes. Because extensive studies have been made with dicopper(II) compounds, some structure−activity correlations have been determined in these systems.[10,12,13b,c,14,15] On the other hand, it has not been possible to propose a correlation in the complexes of other metal ions because of the limited number of studies.

Regarding manganese compounds acting as catalysts for catecholase activity, some mononuclear, dinuclear, and oligonuclear systems are known.[16−19] However, there is no example of the dinuclear $Mn^{III}Mn^{II}$ catalyst. Because the native enzyme contains a dinuclear active center, new dinuclear types of complexes of even the other metal ions, $Mn^{III}Mn^{II}$, for example, deserve more importance in model studies than mononuclear or oligonuclear systems. Dinuclear $Mn^{III}Mn^{II}$ complexes having new types of bridging cores should also be important to explore their magnetic properties.

Robson-type diimino/aminodiphenolate macrocycles are well explored ligands. While a few mixed-valence $Fe^{III}Fe^{II}$ compounds having both phenoxo and carboxylate bridges have been reported derived from such macrocycles[3a,4] and with those interesting results on localization/delocalization have been obtained, no dinuclear $Mn^{III}Mn^{II}$ compound having both phenoxo and carboxylate bridges derived from Robson-type macrocycles is known. Because carboxylate is a suitable leaving group for incoming catecholate moiety to show catecholase activity, such catalytic aspect may be explored with the dinuclear $Mn^{III}Mn^{II}$ compounds having both phenoxo and carboxylate bridges. With the above-mentioned aims, we have prepared three bis(μ-phenoxo)-μ-carboxylate $Mn^{III}Mn^{II}$ compounds, $[Mn^{III}Mn^{II}L(\mu\text{-}O_2CMe)(H_2O)_2](ClO_4)_2\cdot H_2O\cdot MeCN$ (**1**), $[Mn^{III}Mn^{II}L(\mu\text{-}O_2CPh)(MeOH)(ClO_4)](ClO_4)$ (**2**), and $[\{Mn^{III}Mn^{II}L(\mu\text{-}O_2CEt)(EtOH)\}_2(\mu\text{-}O_2CEt)](ClO_4)_3$ (**3**), derived from the Robson-type macrocycle H_2L (Chart 1), which

Chart 1. Chemical structure of H_2L

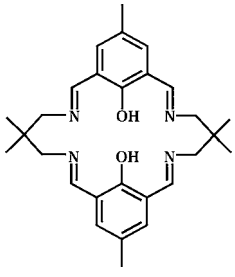

is the [2 + 2] condensation product of 2,6-diformyl-4-methylphenol and 2,2-dimethyl-1,3-diaminopropane. Herein, we report the syntheses, crystal structures, magnetochemistry and theoretical study of the magnetic properties, catecholase activity, and spectroscopy of these three compounds **1**−**3**.

EXPERIMENTAL SECTION

Materials and Physical Measurements. All the reagents and solvents were purchased from commercial sources and used as received. 2,6-Diformyl-4-methylphenol was prepared according to the reported procedure.[21] Elemental (C, H, and N) analyses were performed on a Perkin-Elmer 2400 II analyzer. IR spectra were recorded in the region 400−4000 cm^{-1} on a Bruker-Optics Alpha-T spectrophotometer with samples as KBr disks. Electronic spectra were obtained by using a Shimadzu UV-3600 spectrophotometer. The electrospray ionization mass (ESI-MS positive) spectra were recorded on a Micromass Qtof YA 263 mass spectrometer. Molar conductivity (Λ_M) of 1 mM solution in MeCN and MeOH were measured at 25 °C with a Systronics conductivity bridge. Magnetic susceptibility measurements between 2 and 300 K were carried out in a SQUID magnetometer Quantum Design magnetometer, model MPMP, at the "Unitat de Mesures Magnètiques (Universitat de Barcelona)". Two different magnetic fields were used in all the measurements, 0.05 T (2−30 K) and 1.0 T (2−300 K) for **1** and **3** and 0.02 T (2−30 K) and 0.3 T (2−300 K) for **2**, with superimposable graphs. Pascal's constants were used to estimate the diamagnetic corrections for the compounds.

Syntheses of $[Mn^{III}Mn^{II}L(\mu\text{-}O_2CMe)(H_2O)_2](ClO_4)_2\cdot H_2O\cdot MeCN$ (1), $[Mn^{III}Mn^{II}L(\mu\text{-}O_2CPh)(MeOH)(ClO_4)](ClO_4)$ (2), and $[\{Mn^{III}Mn^{II}L(\mu\text{-}O_2CEt)(EtOH)\}_2(\mu\text{-}O_2CEt)](ClO_4)_3$ (3). These three compounds were prepared following a general procedure as follows: A MeOH solution (5 mL) of 2,2-dimethyl-1,3-diaminopropane (0.102 g, 1 mmol) was added dropwise to a stirred mixture in MeOH (15 mL) containing 2,6-diformyl-4-methylphenol (0.164 g, 1 mmol), manganese(II) perchlorate hexahydrate (0.362 g, 1 mmol), and sodium carboxylate (1 mmol; acetate for **1**, benzoate for **2**, and propionate for **3**). The mixture was stirred for 30 min. The brown colored solution was kept at room temperature for slow evaporation. After a few days, a brown compound that appeared was collected by filtration and dried in vacuum. Recrystallization was done on diffusing diethylether to a solution of **1** in acetonitrile, **2** in methanol, and **3** in ethanol to produce crystalline compounds containing diffraction quality single crystals.

Data for ***1***. Yield: 0.327 g (71%). Anal. Calcd for $C_{32}H_{46}N_5O_{15}Cl_2Mn_2$: C, 41.71; H, 5.03; N, 7.60. Found: C, 41.60; H, 5.25; N, 7.69. Selected FT-IR data on KBr (cm^{-1}): $\nu(H_2O)$, 3425m; $\nu(C{=}N)$, 1633s; $\nu_{as}(CO_2)$, 1570m; $\nu_s(CO_2)$, 1435m; $\nu(ClO_4)$, 1120vs and 626w.

Data for ***2***. Yield: 0.313 g (68%). Anal. Calcd for $C_{36}H_{43}N_4O_{13}Cl_2Mn_2$: C, 46.97; H, 4.71; N, 6.09. Found: C, 47.10; H, 4.50; N, 6.01. Selected FT-IR data on KBr (cm^{-1}): $\nu(C{=}N)$, 1630s; $\nu_{as}(CO_2)$, 1567m; $\nu_s(CO_2)$, 1407m; $\nu(ClO_4)$, 1121vs and 631w.

Data for ***3***. Yield: 0.341 g (78%). Anal. Calcd for $C_{69}H_{95}N_8O_{24}Cl_3Mn_4$: C, 47.45; H, 5.48; N, 6.42. Found: C, 47.30; H, 5.60; N, 6.55. Selected FT-IR data on KBr (cm^{-1}): $\nu(C{=}N)$, 1633s; $\nu_{as}(CO_2)$, 1564m; $\nu_s(CO_2)$, 1433m; $\nu(ClO_4)$, 1121vs and 625w.

Crystal Structure Determination of 1−3. The crystallographic data for **1**, **2**, and **3** are summarized in Table 1. X-ray diffraction data were collected on a Bruker-APEX II SMART CCD diffractometer at 296 K using graphite-monochromated Mo Kα radiation (λ = 0.71073 Å). For data processing, the SAINT[22a] packages were used. All data were corrected for Lorentz-polarization effects. Multiscan absorption correction were made for all three cases using the program SADABS.[22b] Structures were solved by direct and Fourier methods and refined by full-matrix least-squares based on F^2 using SHELXTL[22c] and SHELXL-97 packages.[22d]

During the development of the structures, it became apparent that a few atoms in **1** and **3** were each disordered over two sites or three sites. These disordered atoms were three oxygen atoms, O13, O14, and O15, of a perchlorate moiety in **1** and the following atoms in **3**: two carbon atoms, C33 and C69, of two ethanol molecules; one carbon atom, C36, of a propionate moiety; three oxygen atoms, O13, O14, and O16, of a perchlorate moiety; two oxygen atoms, O18 and O19, of another perchlorate moiety. Except O18 in **3**, which was disordered over three sites, all other disordered atoms were disordered

dx.doi.org/10.1021/ic400916h | Inorg. Chem. 2013, 52, 7732−7746

Table 1. Crystallographic Data for 1−3

	1	2	3
empirical formula	$C_{32}H_{46}N_5O_{15}Cl_2Mn_2$	$C_{36}H_{43}N_4O_{13}Cl_2Mn_2$	$C_{69}H_{80}N_8O_{24}Cl_3Mn_4$
fw	921.52	920.52	1731.52
cryst color	dark red	brown	dark red
cryst syst	monoclinic	monoclinic	monoclinic
space group	$P2_1/c$	$P2_1/n$	$P2_1/n$
a (Å)	19.4432(10)	10.233(4)	12.0581(5)
b (Å)	18.4292(10)	31.236(11)	34.9133(13)
c (Å)	11.7788(6)	12.640(4)	19.5573(7)
α (deg)	90.00	90.00	90.00
β (deg)	104.100(2)	96.002(5)	96.6960(10)
γ (deg)	90.00	90.00	90.00
V (Å^3)	4093.5(4)	4018(2)	8177.2(5)
Z	4	4	4
T (K)	296(2)	296(2)	296(2)
2θ (deg)	2.16−54.70	2.60−52.70	2.34−56.54
μ (mm^{-1})	0.819	0.830	0.777
ρ_{calcd} (g cm^{-3})	1.495	1.522	1.406
$F(000)$	1908	1900	3572
absorp correction	multiscan	multiscan	multiscan
index ranges	$-25 \le h \le 24$	$-12 \le h \le 12$	$-16 \le h \le 14$
	$-22 \le k \le 23$	$-38 \le k \le 38$	$-46 \le k \le 46$
	$-15 \le l \le 15$	$-15 \le l \le 15$	$-26 \le l \le 22$
reflns collected	61914	40156	110381
indep reflns (R_{int})	9226 (0.0493)	8034 (0.1084)	19833 (0.0472)
R_1,[a] wR_2[b] ($I > 2\sigma(I)$)	0.0486, 0.1497	0.0644, 0.1270	0.0597, 0.1712
R_1,[a] wR_2[b] (for all data)	0.0751, 0.1705	0.1568, 0.1636	0.0969, 0.1928

[a] $R_1 = [\sum||F_o| - |F_c||/\sum|F_o|]$. [b] $wR_2 = [\sum w(F_o^2 - F_c^2)^2/\sum wF_o^4]^{1/2}$.

over two sites. The disorder was fixed allowing each individual atom to refine freely, and the final occupancy parameters were set as follows: 0.50 and 0.50 for O13, O14, and O15 in **1** and C33, C69, and C36 in **3**; 0.55 and 0.45 for O19 in **3**; 0.65 and 0.35 for O13, O14, and O16 in **3**; 0.50, 0.25, and 0.25 for O18 in **3**.

The following hydrogen atoms were located from difference Fourier maps: six hydrogen atoms of the three water molecules in **1**, one alcoholic hydrogen atom of the methanol molecule in **2**, and two alcoholic hydrogen atoms of the two ethanol molecules in **3**. Because of the disorder problem, it was not possible to insert the following 15 hydrogen atoms in **3**: 10 hydrogen atoms of two ethanol molecules; 5 hydrogen atoms linked with C35 and C36 of one propionate moiety. All the other hydrogen atoms for the compounds **1**−**3** were inserted on geometrical calculated positions with fixed thermal parameters.

All the nonhydrogen atoms were refined anisotropically. On the other hand, all hydrogen atoms which were either located or inserted were refined isotropically. The final refinement converged at the R_1 ($I > 2\sigma(I)$) values of 0.0486, 0.0644, and 0.0597 for **1**, **2**, and **3**, respectively.

Computational Details. The use of electronic structure calculations based on density functional theory provides an excellent estimation of the exchange coupling constants taking into account the tiny involved energy differences.[23] Since a detailed description of the computational strategy used to calculate the exchange coupling constants in dinuclear and polynuclear complexes is outside the scope of this paper, we will focus our discussion here to its most relevant aspects. Previously, we have published a series of papers devoted to such purpose where more details can be found.[24−27] At a practical level, for the evaluation of the n different coupling constants J_{ij} present in a polynuclear complex, we need to carry out calculations for at least $n + 1$ different spin distributions. Thus, solving the system of n equations obtained from the energy differences, we can obtain the n coupling constants. In case that more than n spin distributions were calculated, a fitting procedure to obtain the coupling constants must be used. In the specific case of dinuclear $Mn^{III}Mn^{II}$ complexes **1** and **2**, the $2J$ value is directly obtained from the energy difference between the high-spin state (parallel alignment of the local spins) and the single-determinant low-spin solution (antiparallel alignment of the local spins), usually called broken-symmetry, divided by $2S_1S_2 + S_1$ term ($S_1 = 2$, $S_2 = 5/2$). For the tetranuclear $Mn^{III}_2Mn^{II}_2$ complex **3**, four spin configurations have been calculated the high spin one, two $S = 5$ solutions by the inversion of the Mn1 and Mn4 (see Figure 3), respectively, and finally, an $S = 0$ solution due to the inversion of Mn1 and Mn2.

In previous studies, we analyzed the effect of the basis set and the choice of the functional on the accuracy of the determination of the exchange coupling constants. Thus, we found that the hybrid B3LYP functional,[28] together with the basis sets proposed by Schaefer et al.,[29] provide J values in excellent agreement with the experimental ones. We have employed a basis set of triple-ζ quality proposed by Schaefer et al. The calculations were performed with the Gaussian09 code[30] using guess functions generated with the Jaguar 7.0 code.[31,32]

RESULTS AND DISCUSSION

Syntheses and Characterization. The macrocyclic mixed-valence $Mn^{III}Mn^{II}$ complexes $[Mn^{III}Mn^{II}L(\mu\text{-}O_2CMe)(H_2O)_2](ClO_4)_2\cdot H_2O\cdot MeCN$ (**1**), $[Mn^{III}Mn^{II}L(\mu\text{-}O_2CPh)(MeOH)(ClO_4)](ClO_4)$ (**2**), and $[\{Mn^{III}Mn^{II}L(\mu\text{-}O_2CEt)(EtOH)\}_2(\mu\text{-}O_2CEt)](ClO_4)_3$ (**3**) are readily obtained from the reaction in which 2:2 template condensation of 2,6-diformyl-4-methylphenol and 2,2-dimethyl-1,3-diaminopropane takes place in presence of 2:2 manganese(II) perchlorate hexahydrate and sodium carboxylate (acetate for **1**, benzoate for **2**, and propionate for **3**). The presence of one Mn^{III} and one Mn^{II} center in **1** and **2**, and two Mn^{III} and two Mn^{II} centers in **3** are evidenced from the elemental analyses accompanied by the balancing of charges. While similar reaction conditions have been maintained in the syntheses of the three compounds, it is interesting that dinuclear compounds have been stabilized

dx.doi.org/10.1021/ic400916h | Inorg. Chem. 2013, 52, 7732−7746

when the carboxylate is acetate (**1**) or benzoate (**2**) but tetranuclear when the carboxylate is propionate (**3**). However, it is difficult to explain why such diferrence takes place; this depends on some subtle effects.

The FT-IR spectra of **1**−**3** reveal the presence of C═N moieties (1633 cm^{-1} in **1** and **3** and 1630 cm^{-1} in **2**), carboxylate (1570 and 1435 cm^{-1} in **1**, 1567 and 1407 cm^{-1} in **2**, and 1564 and 1433 cm^{-1} in **3**), and perchlorate (1120 and 626 cm^{-1} in **1**, 1121 and 631 cm^{-1} in **2**, and 1121 and 625 cm^{-1} in **3**). The difference in energy, 131−160 cm^{-1}, between the antisymmetric and symmetric carboxylate stretching frequencies in **1**−**3** is in line with the bidentate bridging mode.[33]

Electronic spectra (200−1200 nm) of **1**−**3** were recorded in both MeCN and MeOH. In MeCN, four characteristic absorption signals are observed in the spectra of all three complexes: one band at 251 or 252 nm (ε = 48556−73320 M^{-1} cm^{-1}), one shoulder at 284 or 286 nm (ε = 20520−41244 M^{-1} cm^{-1}), one band at 373 or 376 nm (ε = 8080−17160 M^{-1} cm^{-1}), and one band at 562 or 565 nm (ε = 376−738 M^{-1} cm^{-1}). The strongly intense absorptions at 251/252 and 284/286 nm arise due to $\pi \rightarrow \pi^*$ transition of the macrocyclic moiety, while the band at 373/376 nm can be assigned to the phenoxo to Mn^{II}/Mn^{III} ligand to metal charge transfer (LMCT) transition. On the other hand, the band of least intensity at 562/565 nm corresponds to the d−d transition associated with the high-spin Mn^{III} center. In MeOH, the shoulder at 284/286 nm is not observed. Otherwise, the spectra in MeOH are similar to those in MeCN except that the band intensity and maximum are slightly changed.

The molar conductance values at 298 K for **1**−**3** in MeCN are 310, 300, and 410 Ω^{-1} cm^{-1} mol^{-1} L, respectively and in MeOH 180, 180, and 270 Ω^{-1} cm^{-1} mol^{-1} L, respectively. These values indicate that the 2:1 electrolytic nature of **1** and **2** and 3:1 electrolytic nature of **3** in solid state are also retained in both the MeCN and MeOH solutions.[34]

Description of the Structures of $[Mn^{III}Mn^{II}L(\mu\text{-}O_2CMe)(H_2O)_2](ClO_4)_2\cdot H_2O\cdot MeCN$ (1), $[Mn^{III}Mn^{II}L(\mu\text{-}O_2CPh)(MeOH)(ClO_4)](ClO_4)$ (2), and $[\{Mn^{III}Mn^{II}L(\mu\text{-}O_2CEt)(EtOH)\}_2(\mu\text{-}O_2CEt)](ClO_4)_3$ (3). The structures of compounds **1**−**3** are shown in Figures 1−3, respectively. The selected bond lengths and angles of **1** and **2** are listed in Table 2, while those of **3** are listed in Table S1 (Supporting Information). Selected bond lengths and angles and some other structural parameters of the three complexes are compared in Table 3.

Compounds **1** and **2** are dimanganese systems containing one tetraiminodiphenolate macrocyclic ligand L^{2-}, while compound **3** is a tetramanganese compound containing two L^{2-} ligands. In addition to the dianionic organic ligand, L^{2-}, the presence of three monoanionic moieties, two perchlorate anions and one carboxylate anion (acetate in **1** and benzoate in **2**), in **1** and **2** indicate that these two compounds are mixed-valence $Mn^{III}Mn^{II}$ systems. Similarly, the presence of two L^{2-}, three perchlorates, and two propionates indicate that the tetramanganese compound **3** is a $Mn^{III}_2Mn^{II}_2$ system. As described below, the relative bond lengths involving the metal centers and bond valence sum calculations indicate that the Mn1 centers in **1** and **2** are in +III state, while the Mn2 centers in **1** and **2** are in +II state. The same criteria indicate that the Mn1, Mn2, Mn3, and Mn4 centers in **3** are, respectively, in +III, +II, +II, and +III states, and therefore, it is convenient to designate **3** as a $Mn^{III}Mn^{II}Mn^{II}Mn^{III}$ compound.

Each of the two $N(imine)_2O(phenoxo)_2$ compartments of L^{2-} satisfy four coordination positions for a Mn^{III}/Mn^{II} center

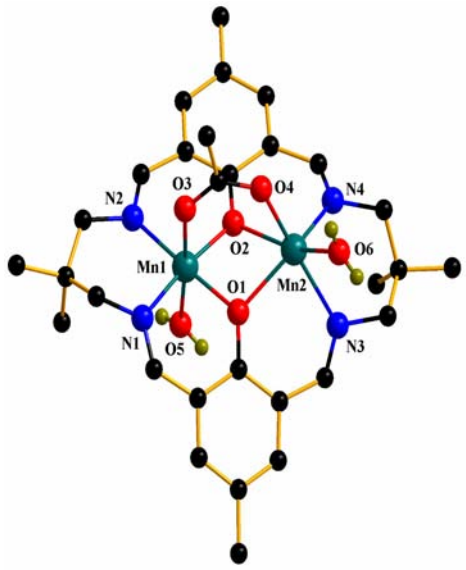

Figure 1. Crystal structure of $[Mn^{III}Mn^{II}L(\mu\text{-}O_2CMe)(H_2O)_2](ClO_4)_2\cdot H_2O\cdot MeCN$ (**1**). All hydrogen atoms except those of coordinated water molecules, two perchlorate ions, one water molecule, and one acetonitrile molecule have been deleted for clarity.

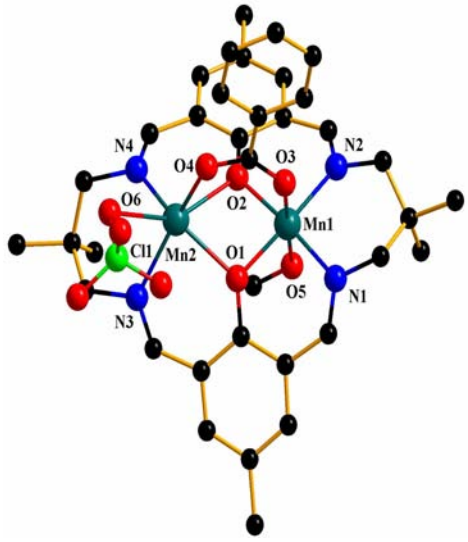

Figure 2. Crystal structure of $[Mn^{III}Mn^{II}L(\mu\text{-}O_2CPh)(MeOH)(ClO_4)](ClO_4)$ (**2**). All hydrogen atoms and one perchlorate ion have been deleted for clarity.

in **1**−**3**. The Mn^{III} and Mn^{II} ions in **1** and **2** and within one L^{2-} in **3** are bridged by the two phenoxo oxygen atoms of L^{2-} and a $\mu_{1,3}$-carboxylate moiety (acetate in **1**, benzoate in **2**, and propionate in **3**); that is, these Mn^{III} and Mn^{II} ions are bridged by a bis(μ-phenoxo)-μ-carboxylate moiety. The Mn^{III} center is hexacoordinated in which the sixth coordination site is occupied by the oxygen atom of a water, methanol, and ethanol molecule in **1**, **2**, and **3**, respectively. The Mn^{II} center is also hexacoordinated in which the sixth coordination site in **1** and **2** is occupied by the oxygen atom of a water molecule and an oxygen atom of a perchlorate moiety, respectively, while the sixth coordination sites of the two Mn^{II} centers within two L^{2-} in **3** are occupied by two oxygen atoms of a bridging propionate moiety, and therefore the compound **3** may be considered as a dimer of two $Mn^{III}Mn^{II}$ dinuclear units.

dx.doi.org/10.1021/ic400916h | Inorg. Chem. 2013, 52, 7732−7746

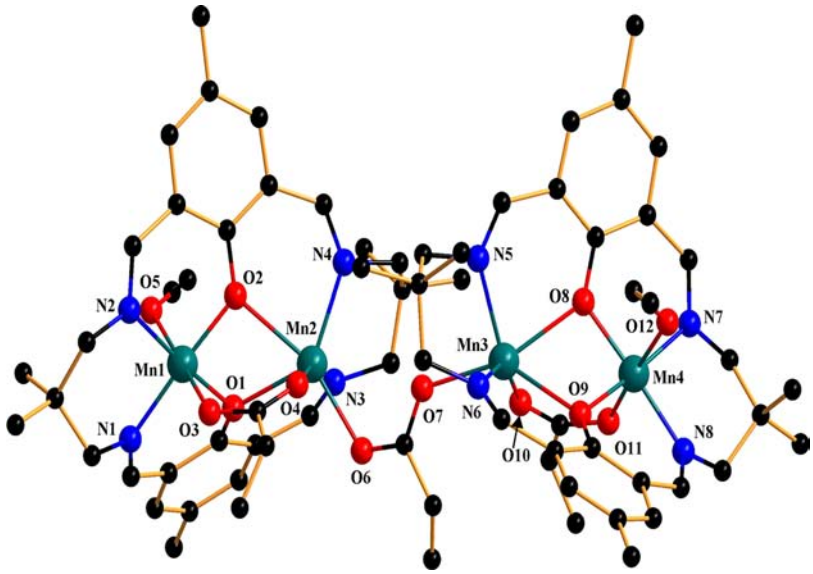

Figure 3. Crystal structure of $[\{Mn^{III}Mn^{II}L(\mu\text{-}O_2CEt)(EtOH)\}_2(\mu\text{-}O_2CEt)](ClO_4)_3$ (**3**). All hydrogen atoms and three perchlorate ions have been deleted for clarity.

Table 2. Selected Structural Parameters (Distances in Å and Angles in deg) of $[Mn^{III}Mn^{II}L(\mu\text{-}O_2CMe)(H_2O)_2](ClO_4)_2\cdot H_2O\cdot MeCN$ (1) and $[Mn^{III}Mn^{II}L(\mu\text{-}O_2CPh)(MeOH)(ClO_4)](ClO_4)$ (2)

bond lengths			bond angles		
	1	2		1	2
Mn1−O1	1.9290(19)	1.916(3)	O1−Mn1−N2	175.63(10)	172.21(17)
Mn1−O2	1.912(2)	1.900(3)	O2−Mn1−N1	171.94(9)	174.78(17)
Mn1−O3	2.118(2)	2.096(4)	O3−Mn1−O5	175.55(9)	177.62(17)
Mn1−O5	2.242(2)	2.316(4)	O1−Mn1−N1	89.56(9)	91.39(16)
Mn1−N1	1.999(2)	1.980(4)	O1−Mn1−O2	82.48(8)	83.41(14)
Mn1−N2	2.021(2)	1.988(5)	O1−Mn1−O3	97.00(9)	96.15(15)
			O1−Mn1−O5	87.44(9)	85.98(16)
			O2−Mn1−N2	93.76(9)	91.70(17)
			O2−Mn1−O3	90.79(9)	92.25(15)
			O2−Mn1−O5	89.99(9)	86.93(16)
			O3−Mn1−N1	88.88(9)	88.74(16)
			O3−Mn1−N2	85.25(9)	90.09(18)
			O5−Mn1−N1	90.95(10)	92.27(17)
			O5−Mn1−N2	90.33(10)	87.70(18)
			N1−Mn1−N2	94.23(10)	93.42(18)
Mn2−O1	2.1583(19)	2.197(3)	O1−Mn2−N3	82.55(8)	81.54(14)
Mn2−O2	2.359(2)	2.355(3)	O1−Mn2−N4	136.30(9)	129.34(15)
Mn2−O4	2.098(2)	2.086(4)	O1−Mn2−O2	68.02(7)	67.71(12)
Mn2−O6	2.210(3)	2.412(4)	O1−Mn2−O4	97.86(8)	96.43(14)
Mn2−N3	2.239(2)	2.234(4)	O1−Mn2−O6	115.12(11)	135.76(14)
Mn2−N4	2.161(2)	2.198(4)	O2−Mn2−N3	116.93(8)	119.58(14)
			O2−Mn2−N4	79.18(8)	77.14(14)
Mn1···Mn2	3.1818(6)	3.1870(13)	O2−Mn2−O4	82.29(8)	80.52(14)
			O2−Mn2−O6	160.55(9)	151.31(14)
			O4−Mn2−N3	158.78(10)	156.25(17)
			O4−Mn2−N4	105.72(9)	112.82(16)
			O4−Mn2−O6	78.27(10)	80.34(15)
			O6−Mn2−N3	82.36(10)	84.73(15)
			O6−Mn2−N4	105.51(12)	90.91(15)
			N3−Mn2−N4	87.69(9)	85.65(16)
			Mn1−O1−Mn2	102.09(8)	101.37(14)
			Mn1−O2−Mn2	95.74(8)	96.42(15)

The coordination geometry of the Mn^{III} centers in **1**−**3** is Jahn−Teller distorted octahedral in which the two imine nitrogen atoms and two bridging phenoxo oxygen atoms define the basal plane. In the coordination environment of the Mn^{III}

dx.doi.org/10.1021/ic400916h | Inorg. Chem. 2013, 52, 7732−7746

Table 3. Comparison of the Selected Structural Parameters (Distances in Å and Angles in deg) of 1−3

	1	2	3[a]
Mn^{III}−O(phenoxo)	1.912(2), 1.9290(19)	1.900(3), 1.916(3)	1.8890(19), 1.919(2); 1.903(2), 1.925(2)
Mn^{II}−O(phenoxo)	2.1583(19), 2.359(2)	2.197(3), 2.355(3)	2.271(2), 2.374(2); 2.297(2), 2.340(2)
Mn^{III}−N(imine)	1.999(2), 2.021(2)	1.980(4), 1.988(5)	1.990(2), 2.000(3); 1.997(2), 2.004(3)
Mn^{II}−N(imine)	2.161(2), 2.239(2)	2.198(4), 2.234(4)	2.206(2), 2.240(3); 2.188(3), 2.231(3)
Mn^{III}−O(carboxylate)	2.118(2)	2.096(4)	2.101(2); 2.100(2)
Mn^{II}−O(carboxylate) intradimer	2.098(2)	2.086(4)	2.124(3); 2.105(3)
Mn^{III}−O(water)	2.242(2)		
Mn^{II}−O(water)	2.210(3)		
Mn^{III}−O(methanol)		2.316(4)	
Mn^{II}−O(perchlorate)		2.412(4)	
Mn^{III}−O(ethanol)			2.341(3); 2.313(3)
Mn^{II}−O(carboxylate) interdimer			2.136(3); 2.161(2)
Mn^{III}: *cisoid* angles	82.48(8)−97.00(9)	83.41(14)−96.15(15)	85.04(9)−94.73(10); 85.15(9)−95.85(10)
Mn^{III}: *transoid* angles	171.94(9)−175.63(10)	172.21(17)−177.62(17)	173.58(10)−179.27(11); 174.25(10)−176.30(10)
Mn^{II}: angles	68.02(7)−160.55(9)	67.71(12)−156.25(17)	67.25(7)−159.20(12); 67.88(7)−147.49(9)
Mn^{III}: $d_{N,O}$[b]	0.029	0.046	0.036; 0.028
Mn^{II}: $d_{N,O}$[b]	0.213	0.119	0.100; 0.047
Mn^{III}: d_{Mn}[c]	0.009	0.058	0.060; 0.053
Mn^{II}: d_{Mn}[c]	0.976	1.025	1.071; 1.025
Mn^{III}−O(phenoxo)−Mn^{II}	95.74(8)and 102.09(8)	96.42(15) and 101.37(14)	96.98(8)and 99.61(9); 98.44(8) and 99.26(9)
Mn^{III}−O···O−Mn^{II}	−147.16	−147.88	−147.64; −150.48
Mn^{III}···Mn^{II}	3.1818(6)	3.1870(13)	3.2081(6); 3.2256(6)
Mn^{II}···Mn^{II}			5.039
δ(phenyl···phenyl)[d]	29.5	55.4	60.4; 61.4

[a]Dimer of dinuclear units, so two different distances and angles. [b]Mean deviation from the least-squares N_2O_2 planes. [c]Displacement from the least-squares N_2O_2 planes. [d]Dihedral angle between two phenyl rings.

centers, the average deviation (0.028−0.046 Å) of the basal atoms and also the displacement (0.009−0.060 Å) of the metal center from the corresponding least-squares $N(imine)_2O(phenoxo)_2$ plane is very small. The ranges of the *cisoid* and *transoid* angles of the Mn^{III} centers are not very different in **1**−**3** and also not deviated much from the ideal values; considering all the Mn^{III} centers in **1**−**3**, the ranges are 82.48(8)−97.00(9)° and 171.94(9)−179.27(11)°, respectively.

On the other hand, the coordination environment of the Mn^{II} centers can be considered as trigonal prism in which the one trigonal plane is constituted by the two phenoxo and one carboxylate oxygen atoms (O4 in **1** and **2**, and O4 and O10 in **3**), while the second plane is defined by the two imine nitrogen atoms and one oxygen atom of water (O6 in **1**) or perchlorate (O6 in **2**) or propionate (O6 and O7 in **3**) moieties. The dihedral angle between the two trigonal planes is 14.65°, 3.72°, and 20.2°/3.4° in **1**, **2**, and 3, respectively. In the Mn^{II} environment, the phenoxo oxygen and imine nitrogen atoms are less planar, the average deviation being in the range 0.047−0.213 Å, and the Mn^{II} center is shifted significantly (by 0.976−1.071 Å) from the least-squares $N(imine)_2O(phenoxo)_2$ plane.

As compared in Table 3, the Mn1(Mn^{III})−O(phenoxo)/Mn4(Mn^{III})−O(phenoxo) bond distances (1.8890(19)−1.9290(19) Å in **1**−**3**) are significantly shorter than the Mn2(Mn^{II})−O(phenoxo)/Mn3(Mn^{II})−O(phenoxo) bond distances (2.1583(19)−2.374(2) Å in **1**−**3**). Similar is the difference between the metal−imine bond distances involving the Mn1(Mn^{III})/Mn4(Mn^{III}) (1.980(4)−2.021(2) Å in **1**−**3**) and Mn2(Mn^{II})/Mn3(Mn^{II}) (2.161(2)−2.240(3) Å in **1**−**3**) centers. From such differences in bond lengths, it is clear that the Mn1/Mn4 centers are in +III state, while the Mn2/Mn3 centers are in +II state. However, such significant difference between the corresponding Mn^{III}−O(carboxylate)/O(water) and Mn^{II}−O(carboxylate)/O(water) bond distances does not take place for two reasons: (i) Jahn−Teller distortion of Mn^{III} centers resulting in increase of the two axial bond distances and (ii) shifting of the Mn^{II} centers toward the fifth and sixth ligands resulting in decrease of these two bond lengths.

The Mn^{III}···Mn^{II} distances in the dinuclear cores in **1** and **2** are almost identical, 3.1818(6) and 3.1870(13) Å, respectively, while that in **3** is only slightly greater, 3.2081(6)/3.2256(6) Å. The Mn^{II}···Mn^{II} distance in **3** is 5.039 Å. Both the smaller and larger Mn^{III}−O(phenoxo)−Mn^{II} angles in **1** and **2** are almost identical but different than the corresponding angles in **3**: 95.74(8)° and 102.09(8)° in **1**, 96.42(15)° and 101.37(14)° in **2**, 96.98(8)° and 99.61(9)° in one unit and 98.44(8)° and 99.26(9)° in the second unit in **3**. However, the average Mn^{III}−O(phenoxo)−Mn^{II} angle in **1**, **2**, and both dinuclear units of **3** are very close (98.91° in **1**, 98.89° in **2**, and 98.29° and 98.85° in **3**). The dihedral angles between the two phenyl rings in **1** (29.5°), **2** (55.4°), and **3** (60.4° and 61.4°) indicate the twisting of the whole molecule to a different extent. The Mn^{III}−O···O−Mn^{II} torsion angles in **1** (−147.16°), **2** (−147.88°), and one unit (−147.64°) in **3** are almost identical, while that in the second unit (−150.48°) of **3** is slightly greater.

We have also performed the bond valence sum (BVS) calculations to assign the oxidation states of the manganese centers.[35] The BVS values are as follows: Mn1 in **1**, 3.06; Mn1 in **2**, 3.17; Mn1 in **3**, 3.12; Mn4 in **3**, 3.09; Mn2 in **1**, 2.03; Mn2 in **2**, 1.85; Mn2 in **3**, 1.92; Mn3 in **3**, 1.95. Clearly, the assignment of Mn^{III} and Mn^{II} centers based on bond distances is in line with the BVS values.

Catecholase Activity. With 3,5-di-*tert*-butyl catechol (3,5-$DTBCH_2$) as the substrate, catecholase activity is usually studied by monitoring UV−vis spectra because the oxidized product, 3,5-di-*tert*-butyl quinone (3,5-DTBQ), has a character-

dx.doi.org/10.1021/ic400916h | Inorg. Chem. 2013, 52, 7732−7746

istic band at ca. 400 nm. To check the ability of complexes **1**−**3** to behave as catalyst for catecholase activity, a 1.0×10^{-5} M solution of a complex was treated with a 100-fold concentrated solution of 3,5-$DTBCH_2$, and the spectra were recorded up to 60 min. Experiments were done in both MeCN and MeOH. It may be noted here that a blank experiment without catalyst does not show formation of the quinone up to 12 h in MeCN and up to 6 h in MeOH.

Spectral changes of the complexes in the presence of 3,5-$DTBCH_2$ are shown in Figure 4 for **1** in MeCN and in Figures S1−S5, Supporting Information, for **1** in MeOH and for **2** and **3** in MeCN and MeOH, respectively. As can be seen from these figures, because of the addition of 3,5-$DTBCH_2$, a band with maximum in the region 385−390 nm is generated and its intensity gradually increases. Clearly, the growing band is due to the formation of 3,5-DTBQ. While the profiles are similar for **1** and **3** in MeCN and MeOH and **2** in MeOH, the profile for **2** in MeCN is different. In the latter case, the initial increase of intensity changes only slightly up to 20 min followed by usual steady increase. However, it is clear from the behavior that all three complexes **1**−**3** show catechol oxidase activity in both MeCN and MeOH.

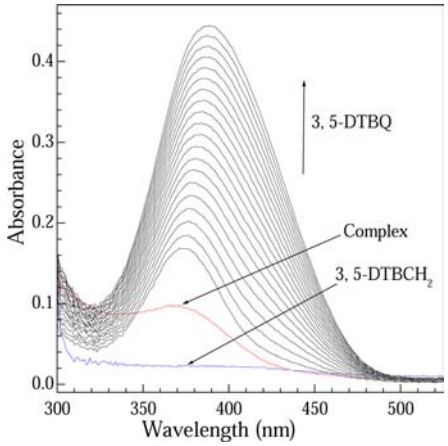

Figure 4. The spectral profile showing the increase of quinone band at 389 nm after the addition of 100-fold 3,5-$DTBCH_2$ to a solution containing complex **1** (1×10^{-5} M) in MeCN. The first spectrum of the complex + 3,5-$DTBCH_2$ mixture was recorded within 1 min after mixing. The next spectra were recorded at 3 min intervals.

As can be seen from Figure 4 and Figures S1−S5, Supporting Information, the spectral profiles starting from the first spectrum of the mixture show consistent change, indicating gradual increase of 3,5-DTBQ concentration. On the other hand, the difference between the optical densities of the first spectrum of the mixture and the spectrum of the complex is rather significant, indicating that the band of 3,5-DTBQ is more intense than the LMCT band. In line with what one can expect, the following general trend (excluding complex **2** in MeCN; *vide supra* also) is also observed: the higher the K_{cat} values (*vide infra*), the greater the increase of the spectrum of the mixture in comparison to that of the complex.

It can also be seen from Figure 4 and Figures S1−S5, Supporting Information, that enhancement of the intensity of the 385−390 nm band is not symmetrical; λ_{max} shifts toward low energy with increasing intensity. This should not happen if the increase in intensity is entirely due to increase in the concentration of 3,5-DTBQ. As already mentioned and shown in Figure 4 and Figures S1−S5, Supporting Information, each of complexes **1**−**3** has a LMCT transition of appreciable intensity at 373/376 nm. In the process of catalyzing the catechol moiety, the composition of the complex should be changed definitely in a cyclic way, but the LMCT transition should be there in all the complex species, and it is also expected that the LMCT band maxima of all such species will be close to 373/376 nm. Thus, it is more probable that both the LMCT transition of complex species and transition of 3,5-DTBQ takes place in the mixture, and the two types of bands are merged since the gap between the two (3,5-DTBQ band at 385−390 nm here; LMCT band at 373/376 nm here) is only 12−17 nm. Eventually, λ_{max} shifts toward low energy with increasing intensity because the 3,5-DTBQ band is more intense than the LMCT band (*vide infra*), and the concentration of 3,5-DTBQ increases gradually.

Kinetic studies were performed to understand the extent of the efficiency. For this purpose, a 1×10^{-5} M solution of a complex was treated with the substrate solution at concentration between 10-fold and 100-fold that of the complex. The experiments were done at a constant temperature of 25 °C under aerobic conditions. For a particular complex−substrate mixture, time scan at the maximum of the quinone band was carried out for a period of 60 min. Because the spectral profile for **2** in MeCN is smooth and steady after 20 min of mixing, the time scan data after 20 min of mixing were considered as the initial data in kinetic studies. For other cases, as usual, data just after mixing were considered. As already discussed, the optical density of 3,5-DTBQ is associated with that of LMCT band of the complex species, so the optical density obtained in the time scan was subtracted by the optical density of the corresponding complex at the wavelength at which time scan was monitored. This difference in optical densities was plotted against time, and the rate constant was determined from that plot by the initial rate method.[36] The rate constants versus concentration of the substrate data were then analyzed on the basis of the Michaelis−Menten approach of enzymatic kinetics to get the Lineweaver−Burk plot, as well as the values of the parameters V_{max}, K_M, and K_{cat}. Th observed and simulated rate constant versus substrate concentration plot and the Lineweaver−Burk plot for complex **1** in MeCN are shown in Figure 5, while the similar plots for other cases are shown in Figures S6−S10, Supporting Information. It may be mentioned that the rate constant versus substrate concentration profile for **2** in MeCN becomes very much zigzag and far from the Michaelis−Menten

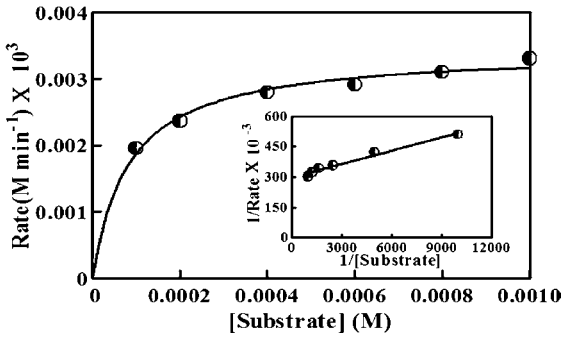

Figure 5. Initial rates versus substrate concentration for the 3,5-$DTBCH_2$→3,5-DTBQ oxidation reaction catalyzed by complex **1** in MeCN. Inset shows Lineweaver−Burk plot. Symbols and solid lines represent the observed and simulated profiles, respectively.

dx.doi.org/10.1021/ic400916h | *Inorg. Chem.* 2013, 52, 7732−7746

Table 4. Kinetic Parameters for Catecholase Activity of 1−3

complex	solvent	V_{max} (M min^{-1})	std. error	K_M (M)	std. error	K_{cat} (h^{-1})
1	MeCN	3.430×10^{-6}	9.339×10^{-8}	0.0000826	0.0000161	20.6
	MeOH	1.931×10^{-6}	1.215×10^{-7}	0.0001573	0.0000370	11.6
2	MeCN	2.601×10^{-6}	3.430×10^{-7}	0.0006265	0.0001672	15.6
	MeOH	1.246×10^{-6}	4.730×10^{-8}	0.0001370	0.0000207	7.5
3	MeCN	1.079×10^{-5}	2.678×10^{-7}	0.0001149	0.0000124	64.7
	MeOH	7.440×10^{-6}	5.178×10^{-7}	0.0004170	0.0000698	44.6

Table 5. The Peak Position, Composition, and Empirical Formula of the Species in the ESI-MS Positive Spectra of 1−3 and Mixture of 1 with 3,5-DTBCH$_2$

composition of species	empirical formula; m/z	**1**	**2**	**3**	**1** + 3,5-DTBCH$_2$
$[H_4L]^{2+}$	$C_{28}H_{38}N_4O_2$; 231.31	50%	12%	40%	
$[Mn^{II}_2L^1]^{2+}$	$C_{23}H_{24}N_2O_4Mn_2$; 251.16	65%	15%	55%	
$[Mn^{IV}L]^{2+}$	$C_{28}H_{34}N_4O_2Mn$; 256.77	100%	60%	45%	95%
$[H_3L]^+$	$C_{28}H_{37}N_4O_2$; 461.63	30%	5%	35%	50%
$[Mn^{III}L]^+$	$C_{28}H_{34}N_4O_2Mn$; 513.54	50%	20%	100%	20%
$[Mn^{III}L(H_2O)]^+$	$C_{28}H_{36}N_4O_3Mn$; 531.56	25%	12%	40%	
$[Mn^{IV}L(carboxylate)]^+$	$C_{30}H_{37}N_4O_4Mn$ for **1**; 572.59	10%	100%	10%	
	$C_{35}H_{39}N_4O_4Mn$ for **2**; 634.66				
	$C_{31}H_{39}N_4O_4Mn$ for **3**; 586.62				
$[Mn^{IV}L(ClO_4)]^+$	$C_{28}H_{34}N_4O_6ClMn$; 613.00	85%		85%	
$[Mn^{II}_2L(\mu\text{-}O_2CMe)(H_2O)]^+$	$C_{30}H_{39}N_4O_5Mn_2$; 645.54	7%			
$[Mn^{III}Mn^{II}L(\mu\text{-}O_2CPh)]^{2+}$	$C_{35}H_{39}N_4O_4Mn_2$; 344.80		6%		
$[3,5\text{-DTBQ-Na}]^+$	$C_{14}H_{20}O_2Na$; 243.30				100%
$[Mn^{III}Mn^{II}L(\mu\text{-}3,5\text{-DTBC}^{2-})]^+$	$C_{42}H_{54}N_4O_4Mn_2$; 788.80				12%

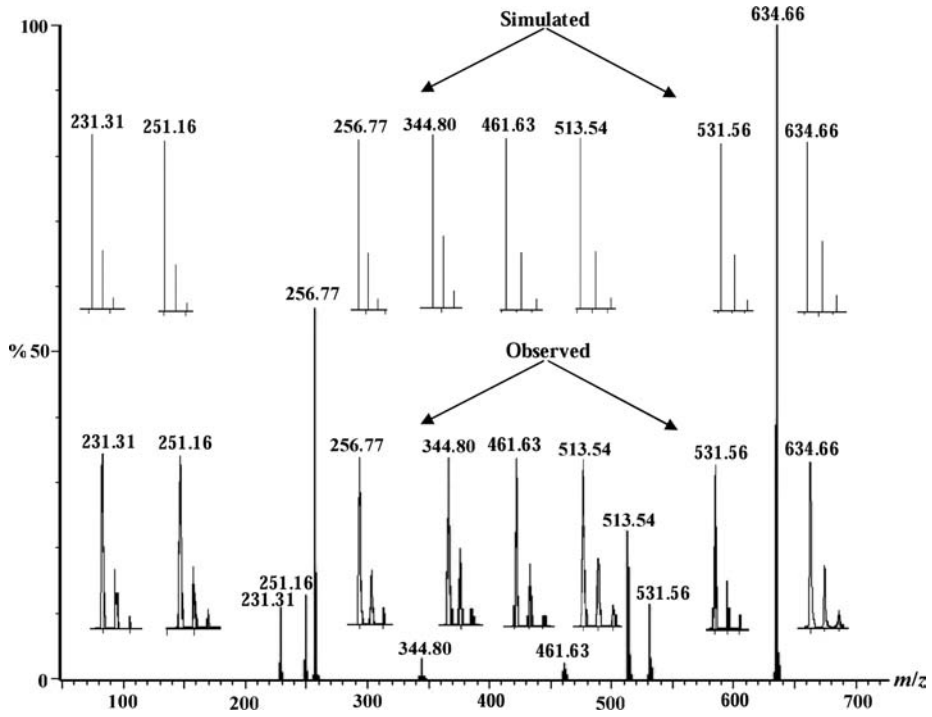

Figure 6. Electrospray ionization mass spectrum (ESI-MS positive) of $[Mn^{III}Mn^{II}L(\mu\text{-}O_2CPh)(MeOH)(ClO_4)](ClO_4)$ (**2**) in MeCN showing observed and simulated isotopic distribution pattern.

model if initial data are taken into consideration. The kinetic parameters for all the cases are listed in Table 4.

As listed in Table 4, the turnover number (K_{cat}) for complexes **1**−**3** in MeCN (20.6, 15.6, and 64.7 h^{-1} for **1**−**3**, respectively) is greater than that in MeOH (11.6, 7.5, and 44.6 h^{-1} for **1**−**3**, respectively). In both the solvents, the order of K_{cat} follows the order **3** (propionate) > **1** (acetate) > **2** (benzoate). Largest K_{cat} value of **3** is probably related to the presence of two dinuclear $Mn^{III}Mn^{II}$ units. On the other hand, the larger K_{cat} value of **1** than **2** is most probably due to the larger steric hindrance of benzoate than acetate for the incoming catechol moiety.[12a,c,d,13a] The different K_{cat} values for a particular compound in two solvents demonstrate the solvent dependency of the phenomena.[12a,e] The solvent

dx.doi.org/10.1021/ic400916h | Inorg. Chem. 2013, 52, 7732−7746

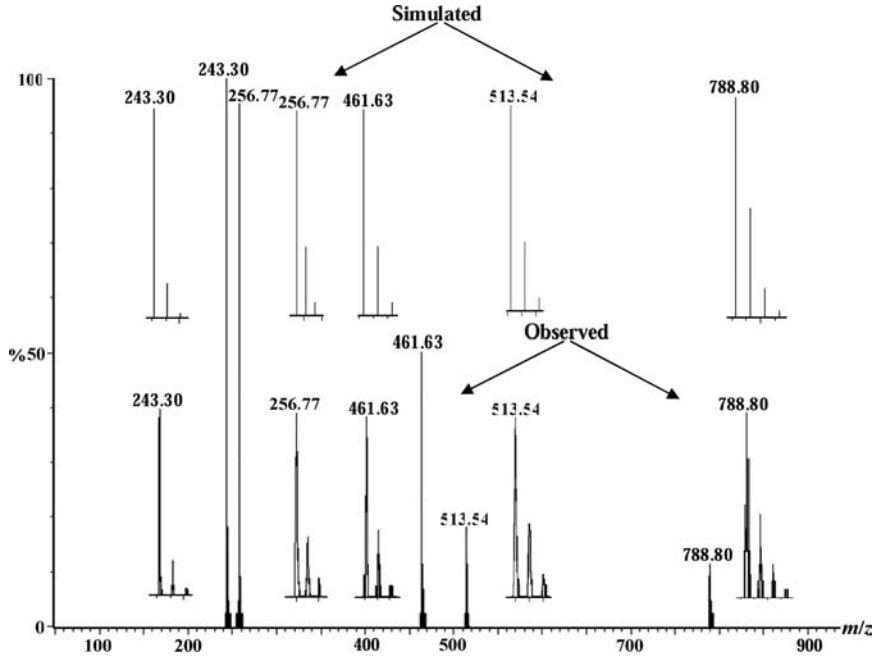

Figure 7. Electrospray ionization mass spectrum (ESI-MS positive) of a 1:100 mixture of $[Mn^{III}Mn^{II}L(\mu\text{-}O_2CMe)(H_2O)_2](ClO_4)_2\cdot H_2O\cdot MeCN$ (**1**) and 3,5-DTBCH$_2$ in MeCN recorded after 15 min of mixing, showing observed and simulated isotopic distribution pattern.

dependency is also reflected for **2**, smooth and steady from the beginning in MeOH but only after 20 min in MeCN. It may be mentioned at this point that the K_{cat} values of the previously reported manganese catalysts lie in a wide range, between very small values like 1.7 h^{-1} and appreciably high values like 1620 h^{-1}.[17b,19] Thus, K_{cat} values of **1**−**3** lie in the ranges as observed previously for other types of manganese catalysts.

Electrospray Ionization Mass Spectral Study. ESI-MS positive spectrum of the MeCN solutions of the complexes **1**−**3** were recorded. To get insight on the nature of a possible complex−substrate intermediate, an ESI-MS positive spectrum of a 1:100 mixture of complex **1** and 3,5-DTBCH$_2$ in MeCN were also recorded after 15 min of mixing. The peak positions, relative peak intensities, and the corresponding assigned cations are listed in Table 5, while observed along with simulated isotopic distribution patterns are demonstrated in Figures 6 (for **2**) and 7 (for **1** + 3,5-DTBCH$_2$) and Figures S11 (for **1**) and S12 (for **3**), Supporting Information.

As listed in Table 5, some species are monocationic, while some others are dicationic for which line-to-line separation of, respectively, 1.0 and 0.5 was observed. Seven peaks are common in the spectra of **1**−**3**. These are assignable to the following species: (i) dicationic organic cation $[H_4L]^{2+}$ and monocationic organic cation $[H_3L]^+$; (ii) mononuclear manganese(III) species $[Mn^{III}L]^+$ and $[Mn^{III}L(H_2O)]^+$; (iii) mononuclear manganese(IV) species $[Mn^{IV}L]^{2+}$ and $[Mn^{IV}L\text{-}(carboxylate)]^+$ (carboxylate = acetate, benzoate, and propionate for **1**, **2**, and **3**, respectively); (iv) dimanganese(II) species $[Mn^{II}_2L^1]^{2+}$, where H_2L^1 is a decomposed product of the parent ligand and the 2:1 condensation product of 2,6-diformyl-4-methylphenol and 2,2-dimethyl-1,3-diaminopropane. In addition to $[Mn^{IV}L]^{2+}$ and $[Mn^{IV}L(carboxylate)]^+$, one more manganese(IV) species, $[Mn^{IV}L(perchlorate)]^+$, also appeared in the spectra of **1** and **3**. Again, in addition to $[Mn^{II}_2L^1]^{2+}$, one more dimanganese(II) species, $[Mn^{II}_2L(\mu\text{-}O_2CMe)(H_2O)]^+$, also appeared in the case of **1**. As in the original compounds, a mixed-valence $Mn^{III}Mn^{II}$ species $[Mn^{III}Mn^{II}(\mu\text{-}O_2CPh)]^{2+}$ is observed in the spectrum of **2**.

Five peaks appeared in the spectrum of 1:100 mixture of complex **1** and 3,5-DTBCH$_2$ (Figure 7). Three among them correspond to the three species $[H_3L]^+$, $[Mn^{III}L]^+$, and $[Mn^{IV}L]^{2+}$, which are among those appearing in the spectrum of the original compound **1**. One (at m/z = 243.30) of the remaining two peaks is well assignable to the quinone-sodium aggregate $[3,5\text{-DTBQ-Na}]^+$. The remaining peak at m/z = 788.80 is quite interesting because the peak position, line-to-line separation, and matching of the isotopic distributions of the observed and the simulated patterns (Figure 7) clearly indicate that this peak arises due to 1:1 complex−substrate aggregate $[Mn^{III}Mn^{II}L(\mu\text{-}3,5\text{-}DTBC^{2-})]^+$.

Magnetic Properties of 1 and 2. The magnetic behavior of **1** and **2** was recorded, and their resulting $\chi_M T$ versus T plots are depicted in Figure 8. Both compounds display weak intramolecular interactions, which clearly differ in their nature despite the similarities between both species. Indeed, at 300 K, $\chi_M T$ products of 7.76 $cm^3\ mol^{-1}\ K$ (**1**) and 7.54 $cm^3\ mol^{-1}\ K$ (**2**) were found, values in the range expected for dinuclear systems containing uncoupled Mn^{III} (S = 2) and Mn^{II} centers (S = 5/2), 7.38 $cm^3\ mol^{-1}\ K$ when g = 2.0. In the course of cooling, $\chi_M T$ remains almost constant for **1** between 300 and 50 K; it is smoothly decreasing for **2** in the same range. Then, the following main changes appear: compound **1** reaches a maximum at 11.0 K (of 7.88 $cm^3\ mol^{-1}\ K$) dropping to 7.15 $cm^3\ mol^{-1}\ K$ at 2 K, whereas $\chi_M T$ of compound **2** continues falling faster arriving finally at 4.15 $cm^3\ mol^{-1}\ K$ (at 2 K). The faster decrease in the low temperature region for both the compounds is due to the presence of magnetic anisotropy zero-field splitting (quite remarkable in Mn^{III} centers), the effect of intermolecular interactions, or both. However, the shape of the graphs indicate intramolecular ferromagnetic coupling between the Mn^{III} and Mn^{II} centers in **1** and antiferromangetic exchange in the case of compound **2**.

dx.doi.org/10.1021/ic400916h | Inorg. Chem. 2013, 52, 7732−7746

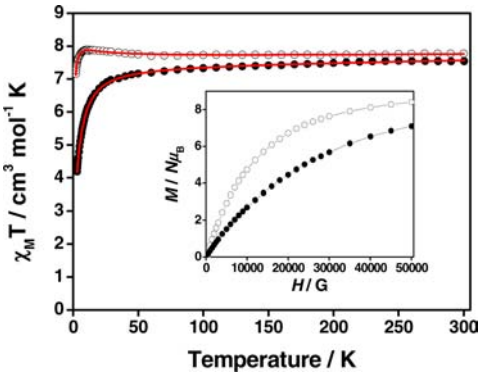

Figure 8. $\chi_M T$ vs T plots for $[Mn^{III}Mn^{II}L(\mu\text{-}O_2CMe)(H_2O)_2](ClO_4)_2\cdot H_2O\cdot MeCN$ (**1**) and $[Mn^{III}Mn^{II}L(\mu\text{-}O_2CPh)(MeOH)(ClO_4)](ClO_4)$ (**2**) between 2 and 300 K. The experimental data are shown as open (**1**) and filled (**2**) spheres, and the red lines correspond to their theoretical values. Inset shows $M/(N\mu_B)$ vs H/G plots of **1** and **2** following the same legend.

As discussed, both species **1** and **2** contain one Mn^{III} and one Mn^{II} center in which the Mn^{II} center is highly distorted from the ideal octahedral geometry, whereas the Mn^{III} center displays clear Jahn–Teller elongation perpendicular to L^{2-}, and therefore local anisotropy of Mn^{III} should have a role in the magnetic properties (anisotropic parameters for the Mn^{II} are normally very small). $\chi_M T$ versus T data for **1** and **2** were fitted using the program MAGPACK-fit,[37] in which the exchange spin Hamiltonian is expressed as $H = -2\sum J_{ij}S_iS_j$ and which allows the addition of anisotropic parameters for the Mn^{III} centers (local D and E values). By this method, the best fitting parameters were the following: $2J = +0.16$ cm^{-1}, $g = 2.04$, $|D_{Mn^{III}}| = 3.53$ cm^{-1}, $|E_{Mn^{III}}| = 0.48$ cm^{-1}, and TIP $= 288 \times 10^{-6}$ cm^3 mol^{-1} for compound **1** and $2J = -0.19$ cm^{-1}, $g = 2.00$, $|D_{Mn^{III}}| = 2.65$ cm^{-1}, $|E_{Mn^{III}}| = 0.85$ cm^{-1}, and TIP $= 590 \times 10^{-6}$ cm^3 mol^{-1} for compound **2**. R values of 4×10^{-6} and 6×10^{-6} were found for the compounds, respectively. Based on these parameter values, information about ground state and first excited state have been provided in Supporting Information.

$M/N\mu_B$ vs H/G data for **1** and **2** are shown for comparative reasons in the inset of Figure 8; the shape of both the graphs resemble well other systems that show ferromagnetic (**1**, open spheres) and antiferromagnetic (**2**, filled spheres) behavior, where the values of **1** are always higher than **2**, and no saturation point is reached by the latter. The theoretical saturation value for a dinuclear $Mn^{III}Mn^{II}$ complex, without taking into account other parameters, is calculated to be $9N\mu_B$. In both the compounds, **1** and **2**, the final values are lower and fairly arriving to saturation. This implies the existence of D parameters in both compounds; the values for the local D (and also E) obtained with the fitting of the experimental data, are in the range of the mononuclear Mn^{III} clusters displaying elongated Jahn–Teller distortion.[5h,38] In principle, it may be expected to find a negative zero-field splitting parameter in **1** and **2**, but in our interpretation, such a conclusion could not be assessed.[39]

It should be stressed that additional factors have been overlooked because of overparametrization. This way, intermolecular interactions have not been taken into account, as well as the $D_{Mn^{II}}$ parameter, which in principle must be a small value, although it depends greatly on the coordination number and surroundings of the Mn^{II} ion (indeed, these two species present Mn^{II} centers coordinated to N- and O-ligands displaying a remarkably distorted geometry).[40] Nevertheless, it is evident from Figure 8 that the fits are quite good and calculated values agree well with others in the literature.

Exchange couplings, J, of **1** and **2** are very similar in value (the two species display very weak intramolecular interactions), although they differ in sign (being in agreement with their respective graphs, see Figure 8). In general, $Mn^{III}Mn^{II}$ compounds display weak interactions that can be either ferro- or antiferromagnetic in nature.[5a,41−44] Because they have the bis(μ-phenoxo)-μ-carboxylate bridging moiety, the available magnetic pathways for both compounds **1** and **2** are through two oxygen atoms from the phenoxo groups and two oxygens from a carboxylate bridge. Although the *syn*–*syn* mode of bridging carboxylate efficiently provides antiferromagnetic interaction,[45] the effect of such interaction in both **1** and **2** should be reduced because the Jahn–Teller elongation of the Mn^{III} center appears in the direction of the carboxylate. It has been already discussed that the structural parameters like Mn^{III}–O(phenoxo), Mn^{II}–O(phenoxo), Mn^{III}–O(carboxylate), and Mn^{II}–O(carboxylate) distances, $Mn^{III}\cdots Mn^{II}$ distance, Mn^{III}–O(phenoxo)–Mn^{II} angles, and even the Mn^{III}–O(phenoxo)···O(phenoxo)–Mn^{II} torsion angles in **1** and **2** are only slightly different (Tables 2 and 3). On the other hand, the conformation of the two compounds is slightly different (Tables 2 and 3), modifying probably the overlap between the orbitals involved in the exchange. Overall, the weakness of the interactions make the assessment of the main contribution difficult, and at this point the uncertainty of overlooking one factor from the rest should be stressed. To confirm and further analyze the exchange interactions, we have also performed electronic structure calculations, as described below.

The calculated J values obtained using DFT methods (B3LYP functional and triple-ξ all electron basis set, see Computational Details) reproduce properly the sign and the weak strength of the exchange interactions found experimentally. Thus, calculated $2J$ values are +1.2 and −1.9 cm^{-1} for **1** and **2**, respectively, while the experimentally fitted corresponding values are +0.16 and −0.19 cm^{-1}. The bridging ligands are a double phenoxo group of the Robson-type macrocyclic ligand and an axial carboxylate ligand. To check the role of the carboxylate ligand in the magnetic properties, we repeated the calculations for **1** replacing the carboxylate ligand by non-bridging hydroxo and water ligands obtaining a $2J$ value of +1.3 cm^{-1}, practically identical to that obtained in the original complex. In these two systems, the Jahn–Teller axis of the Mn^{III} cation is pointing toward one of the bridging oxygen atoms of the carboxylate ligand (Mn–O distance around 2.1 Å, dotted line in Scheme 1). Hence, such ligands have a minor function in the exchange coupling.

Usually, the main structural parameter in phenoxo-bridged complexes that controls the exchange coupling interactions is the bridging M–O–M angles; however, in this case as mentioned above, the values are almost identical (see Table 6), and they cannot justify the different nature of the exchange interactions in **1** and **2**. In these two systems, Mn^{II} cations have a long Mn–O distance with one of the bridging oxygen atoms of the phenoxo ligands (Mn–O distance longer than 2.3 Å, hashed line in Scheme 1). The analysis of the two structures reveals some differences: (i) In **1** there are two water terminal ligands, while in complex **2**, one water molecule is replaced by a methanol molecule and the second water molecule is replaced by a perchlorate anion. The bridging ligand is acetate in **1** but

dx.doi.org/10.1021/ic400916h | Inorg. Chem. 2013, 52, 7732−7746

Scheme 1. Jahn–Teller Axis (Dotted Line) of Complex 1 or 2

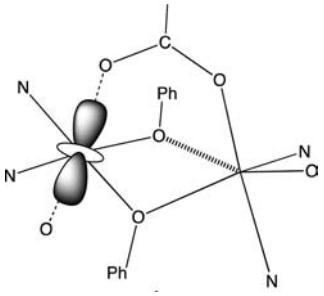

benzoate in **2**. In order to check which modification is responsible for the different sign in the exchange interactions, the complex **2** was calculated by replacing both the perchlorate anion and methanol molecule by water molecules and the benzoate ligand by an acetate ligand, leading to an even more antiferromagnetic 2*J* value of −2.2 cm^{-1}. Thus, these ligand changes cannot justify the ferromagnetic coupling found in **1**. (ii) The Robson-type macrocycle adopts a more planar conformation in complex **1** than in complex **2**. This fact can be evidenced by the O···O–C angles of the bridging ligands, being 151.7° and 177.1° for **1** and 150.5° and 155.5° for **2**. However, this large O···O–C angle (177.1°) of the bridging ligand present in **1** corresponds to the phenoxo bridging ligand showing a long Mn^{II}–O distance (2.359 Å); hence, we can expect that will have a small influence in the exchange coupling (*vide infra* also, discussion of magnetic properties of compound **3**). (iii) There are some differences in the phenoxo Mn^{III}–O distances, 1.929 and 1.916 Å for **1** and **2**, respectively, in the exchange pathway with shorter Mn^{II}–O distances (2.158 Å for **1** and 2.197 Å for **2**; see Scheme 1 and Table 6). The larger Mn^{III}–O distance in **1** (1.929 Å) could be in agreement with the ferromagnetic coupling, and the reduction of such distance will result in complex **2** (1.916 Å) in a larger overlap between the magnetic orbitals in concordance with the antiferromagnetic coupling found experimentally.

The spin density for the ferromagnetic state of complex **1** is shown in Figure 9. The Mn^{II} cation (right in Figure 9) shows

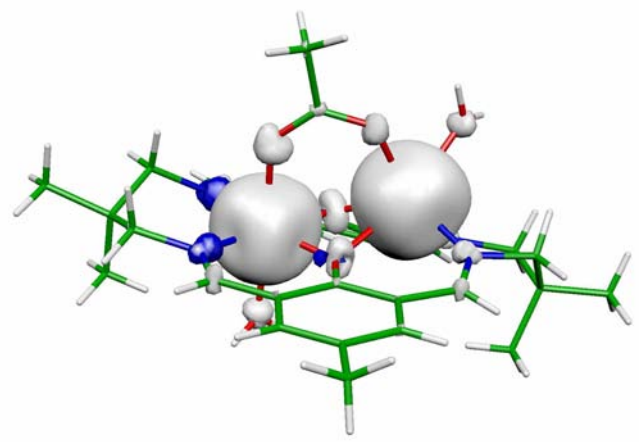

Figure 9. Spin density map for the more stable spin distribution of the ferromagnetic ground state of complex **1**, calculated with the B3LYP functional. The isodensity surface represented corresponds to a value of 0.005 $e^-/bohr^3$ (white regions indicate positive spin populations; negative values are in blue color).

an almost spherical spin distribution, and the presence of unpaired electrons in all the d orbitals leads to a predominance of the spin delocalization resulting in all the neighboring coordinated atoms having spin density with the same sign.[46,47] However, in the Mn^{III} cation (left in Figure 9), the spin distribution is less spherical. The axial Jahn–Teller effect causes the the $d_{x^2-y^2}$ orbital to be empty; thus, in the equatorial plane, the first neighboring atoms have the opposite sign because spin polarization is the predominant mechanism.

Magnetic Properties of Compound 3. This system exhibits a behavior characteristic of very weakly coupled Mn species (Figure S13, Supporting Information). The $\chi_M T$ value at 300 K was found to be 14.60 $cm^3\ mol^{-1}$ K, very close to the expected value (14.75 $cm^3\ mol^{-1}$ K) for an uncoupled tetranuclear $Mn^{III}_2Mn^{II}_2$ system with $S(Mn^{III})$ = 2 and $S(Mn^{II})$ = 5/2 assuming g = 2.00. The $\chi_M T$ value varies slightly from the highest temperatures until approximately 50 K (14.00 $cm^3\ mol^{-1}$ K), then dropping faster to a value of 8.45 $cm^3\ mol^{-1}$ K at 2 K. In **3**, in addition to the interaction between

Table 6. Structural Parameters (Distances in Å and Angles in deg) and Experimental and Calculated $Mn^{III}Mn^{II}$ Exchange Coupling Constants (cm^{-1}) of Macrocyclic $Mn^{III}Mn^{II}$ Compounds 1–3 and Those of the Previously Reported Compounds I and II[41]

	longer Mn^{II}–O pathway					
	Mn^{II}–O	Mn^{III}–O	O···O–C	Mn–O–Mn	Mn^{III}···Mn^{II}	Mn–O···O–Mn
1	2.359	1.912	177.1	95.7	3.182	147.2
2	2.355	1.900	155.5	96.4	3.187	147.9
3, unit I	2.374	1.889	153.6	97.0	3.208	147.6
3, unit II	2.340	1.903	150.9	98.4	3.226	150.5
I	2.386	1.941	163.2	93.6	3.168	145.8
II	2.435	1.905	164.9	97.8	3.290	170.2
	shorter Mn^{II}–O pathway					
	Mn^{II}–O	Mn^{III}–O	O···O–C	Mn–O–Mn	J_{exp}	J_{calc}
1	2.158	1.929	151.7	102.1	+0.08	+0.60
2	2.197	1.916	150.5	101.4	−0.095	−0.95
3, unit I	2.271	1.919	146.9	99.6	+0.015	−1.95
3, unit II	2.297	1.925	147.7	99.3	+0.015	+0.45
I	2.129	1.931	161.8	102.5	−1.8	−0.99
II	2.355	1.911	158.3	100.4	+1.47	+3.45

dx.doi.org/10.1021/ic400916h | *Inorg. Chem.* 2013, 52, 7732–7746

the Mn^{III} and Mn^{II} centers in two dinuclear units, interaction is also possible between the two dinuclear units (interaction between the two Mn^{II} centers) through the carboxylate bridge in a *syn*−*anti* conformation.[38] The experimental magnetic data were fitted using the same program mentioned before, taking into account two intramolecular interactions, J_1 for the exchange within each dinuclear unit and J_2 for the magnetic interaction between the two dinuclear units. The best fit parameters for the studied molecule are $2J_1 = +0.03$ cm^{-1}, $2J_2 = -0.40$ cm^{-1}, $g = 1.99$, and $|D_{Mn^{III}}| = 0.05$ cm^{-1}, and $R = 3 \times 10^{-4}$. Based on these parameter values, information about ground state and first excited state have been provided in Supporting Information.

For the tetranuclear $Mn^{III}_2Mn^{II}_2$ complex **3**, employing the same theoretical approach as for dinuclear complexes (see Computational Details), the exchange coupling constants have been determined. We considered three different J values, two $Mn^{III}\cdots Mn^{II}$ interactions (see Figure 3, J_1 with $d(Mn^{III}\cdots Mn^{II}) = 3.208$ Å and J_1' with $d(Mn^{III}\cdots Mn^{II}) = 3.226$ Å), taking into account the lack of symmetry of the complex, and the central $Mn^{II}\cdots Mn^{II}$ interactions J_2. The calculated $2J$ value for the two first interactions are -3.9 cm^{-1} ($2J_1$) and $+0.9$ cm^{-1} ($2J_1'$) for the $Mn^{III}\cdots Mn^{II}$ interactions, while the *syn*−*anti* carboxylate $Mn^{II}\cdots Mn^{II}$ $2J_2$ value is -0.98 cm^{-1}. The DFT calculated $Mn^{II}\cdots Mn^{II}$ J value agrees with the weak antiferromagnetic coupling experimentally found. Concerning the $Mn^{III}\cdots Mn^{II}$ interactions, theoretical methods easily allow us to consider two different interactions giving two exchange constants of different nature. However, in the fitting procedure, the inclusion of an additional J value complicates the process and increases the possibility of an overparametrization taking into account the small J values involved in such interactions. Thus, from the fitting with a single average J value for the two $Mn^{III}\cdots Mn^{II}$ interactions, a weak ferromagnetic interaction was obtained.

The structural analysis indicates for the two $Mn^{III}\cdots Mn^{II}$ exchange pathways in **3** that the O···O−C angles are closer to those of complex **2** (see Table 6, 146.9° and 153.6° for J_1 and 147.7° and 150.9° for J_1'). Thus, the presence of similar O···O−C angles seems to corroborate that such structural parameter is not crucial to explain the different sign found in the interactions in **3**. Also, a large O···O−C angle is present in the ferromagnetic complex **1**. However, the analysis of the differences in the phenoxo Mn^{III}−O distances, 1.919 and 1.925 Å for J_1 and J_1', respectively, for exchange pathways with shorter Mn^{II}−O distances (2.271 and 2.297 Å, respectively; see Table 6) is in agreement with the results found for **1** and **2**. Thus, it seems that the nature of the exchange interaction is mainly controlled by the exchange pathway including the shorter Mn^{II}−O distances.

It is observed, following Table 6 and comparing compound **3** with **1** and **2**, that the dinuclear units in the three compounds present similar structural parameters. Above it has been seen that intramolecular interactions between the Mn^{III} and Mn^{II} centers in this family of compounds are very weak and could be ferro- or antiferromagnetic. From the fitting it can be estimated that the intramolecular interaction between Mn^{III} and Mn^{II} ions is almost zero ($J_1 = +0.015$ cm^{-1}) the one between the two Mn^{II} centers being the strongest ($J_1 < J_2$). Overall, compound **3** seems to share more similarities with **2** than **1**; both show antiferromagnetic interaction. Despite that, the most remarkable difference between **3** and the other two compounds is the low value of the local zero-field splitting parameter. In **3**, this value is quite low (<0.1 cm^{-1}) in contrast to the values found for **1** (3.53 cm^{-1}) and **2** (2.65 cm^{-1}). This could be nicely explained by the opposite disposition of the Jahn−Teller axes of the two Mn^{III} centers within the system (almost perpendicular, see Figure S14, Supporting Information) canceling each other. In this sense, it is well-known that final arrangements of Jahn−Teller axes can provide remarkable changes in the magnetic behavior of molecular magnets.[5f,g,48]

Comparison of the Synthetic Methodology, Composition, Structure, and Properties of 1−3 with Relevant Systems. Derived from acyclic dinucleating ligands having monophenoxo bridging ability, a number of dinuclear μ-phenoxo-bis(μ-carboxylate) $Mn^{III}Mn^{II}$ compounds have been reported.[42,43] These compounds have been synthesized on reacting the preorganized dinucleating ligand with either manganese(II) acetate and sodium perchlorate or manganese(II) perchlorate and sodium carboxylate. Clearly, a part of manganese(II) undergoes aerial oxidation to yield the $Mn^{III}Mn^{II}$ products. Regarding the dinuclear $Mn^{III}Mn^{II}$ compounds derived from Robson-type dinucleating macrocyclic ligands, there are only two structurally characterized examples. One of them, which is derived from the symmetric macrocyclic ligand H_2L^2 (H_2L^2 = 2:2 condensation product of 2,6-diformyl-4-*tert*-butylphenol and 1,3-diaminopropane), has been synthesized on electrochemical oxidation of a dimanganese(II) compound.[41a] The second macrocyclic example, on the other hand, has been prepared on template condensation of 2,6-diformyl-4-methylphenol and *N*,*N*-bis(2-aminoethyl) glycine in the presence of manganese(II) perchlorate.[41b] However, the aerial oxidation of a part of Mn^{II} to Mn^{III} is accompanied by the group elimination reaction of *N*,*N*-bis(2-aminoethyl) glycine to produce ethylenediamine, and subsequently the product is a $Mn^{III}Mn^{II}$ compound derived from an asymmetric macrocycle. In contrast, the bis(μ-phenoxo)-μ-carboxylate $Mn^{III}Mn^{II}$ compounds **1** and **2** derived from a symmetric macrocyclic ligand, H_2L, are synthesized by template condensation of 2,6-diformyl-4-methylphenol and 2,2-dimethyl-1,3-diaminopropane in presence of manganese(II) perchlorate and sodium carboxylate, that is, **1** and **2** are synthesized following basically the methodology to synthesize μ-phenoxo-bis(μ-carboxylate) $Mn^{III}Mn^{II}$ systems in acyclic dinucleating ligands. Again, while the only two previously reported $Mn^{III}Mn^{II}$ compounds in Robson-type macrocycles are either diphenoxo bridged or bis(μ-phenoxo)-μ-chloro bridged, compounds **1** and **2** are not only the sole examples of bis(μ-phenoxo)-μ-carboxylate $Mn^{III}Mn^{II}$ systems derived from such macrocyclic ligands but also the sole examples of dinuclear $Mn^{III}Mn^{II}$ systems having such bridging core. Structural parameters indicate that the two manganese centers in **1**, **2**, and each of the two dinuclear units of **3** belong to different oxidation states, III for one and II for the second. Magnetic data agree very well with the crystallographic data and corroborate the idea of being a valence-trapped system. So, compounds **1** and **2** represent a new family of valence-trapped dinuclear $Mn^{III}Mn^{II}$ compounds. Compound **3** may be considered as remarkably interesting because of the formation of a dimer of dinuclear cores.

As already mentioned, the exchange interactions between Mn^{III} and Mn^{II} should be weak ferro- or antiferromagnetic. A magneto-structural correlation has been previously proposed on studying the magnetic properties of dinuclear μ-phenoxo-bis(μ-carboxylate) $Mn^{III}Mn^{II}$ compounds in dinucleating acyclic ligands.[43] All of those compounds exhibit weak antiferromagnetic interactions; J lies between −4.1 and −7.7

dx.doi.org/10.1021/ic400916h | Inorg. Chem. 2013, 52, 7732−7746

cm^{-1}. According to this correlation, J is a function of asymmetry of Mn^{III}−O(phenoxo) and Mn^{II}−O(phenoxo) bond distances, the greater the asymmetry, the lower the antiferromagnetic interaction.[43] The magnetic exchange interaction between Mn^{III} and Mn^{II} in the previously published macrocyclic $Mn^{III}Mn^{II}$ compounds, with J values −1.8 (complex **I**) and +1.47 cm^{-1} (complex **II**),[41] and also in **1** (+0.08 cm^{-1}), **2** (−0.095 cm^{-1}), and **3** (+0.015 cm^{-1}) are weakly ferro- or antiferromagnetic. Calculated DFT J values properly reproduce the different nature of these two macrocyclic complexes **I** and **II** (see Table 6). Due to significant difference in the bridging core (particularly one bridging phenoxo in the acyclic systems versus two in **1**/**2**/**3**/**I**/**II**), the correlation in the acyclic systems should not be valid in the macrocyclic complexes; in fact, no correlation is found between the J values and the asymmetry in bond distances in either of the two phenoxo routes (Table 6). There is no unique structural parameter that controls the nature of the exchange interaction for this family of macrocylic $Mn^{III}Mn^{II}$ compounds, and probably, there is subtle interplay of different structural factors. Despite such difficulties, it is worth mentioning that the Mn^{III}−O distances of the exchange pathway including the shorter Mn^{II}−O distances seem to play an important role. Thus, the complexes showing ferromagnetic coupling have either the long Mn^{II}−O distances (see Table 6, **II** and unit II in **3**) or long Mn^{III}−O distances (**1**), but in the case of the complex **I**, despite the long Mn^{III}−O distance, the shortest Mn^{II}−O distance results in antiferromagnetic coupling.

As mentioned, a few dinuclear manganese compounds are known to exhibit catecholase activity. These compounds are bis(μ-oximato)Mn^{II}_2, bis(μ-oxo)Mn^{III}_2, and bis(μ-oxo)Mn^{IV}_2 systems, as well as Mn^{IV}_2 systems having no bridging ligand between the metal centers.[16b,17,19] Clearly, in terms of both bridging moiety and oxidation states of the metal ions, the dinuclear bis(μ-phenoxo)-μ-carboxylate $Mn^{III}Mn^{II}$ compounds **1** and **2** are new examples of catalysts for catechol oxidase activity. Being a dimer of the bis(μ-phenoxo)-μ-carboxylate $Mn^{III}Mn^{II}$ moieties, compound **3** can also be included in this new family.

It is quite essential that the catechol moiety should be coordinated to the metal center of a complex catalyst. Complex−substrate aggregates having 1:1 stoichiometry and having either a monodentate asymmetric coordination or a simultaneous coordination of the substrate to both copper centers in dinucleating bridging fashion is suggested in the two proposed mechanisms regarding the in vivo cycle of the dicopper(II) metallo-enzyme.[11a,c] In the model studies with the dicopper(II) complexes, a few complex−substrate aggregates having 1:1 or 1:2 stoichiometry have been identified crystallographically[15c,d] or from ESI-MS positive spectral studies;[12a] the catechol moieties in these cases are either monodentate/chelating to one copper(II) center or bridging bidentate to both the copper(II) centers. In the manganese catalysts, only a few complex−substrate aggregates that are known have been identified crystallographically, and those involve mononuclear Mn^{II}/Mn^{III} centers; the aggregates have 1:1 stoiochiometry.[16a,17a] In contrast to the previous aggregates identified crystallographically and derived from mononuclear catalysts only, the aggregate $[Mn^{III}Mn^{II}L(\mu\text{-}3,5\text{-}DTBC^{2-})]^+$ in the present investigation has been identified from ESI-MS positive spectrum and is generated from a dimanganese catalyst $[Mn^{III}Mn^{II}L(\mu\text{-}O_2CMe)(H_2O)_2](ClO_4)_2{\cdot}H_2O{\cdot}MeCN$ (**1**). Although complex **1** is not a $Cu^{II}Cu^{II}$ but a $Mn^{III}Mn^{II}$ system, the 1:1 complex−substrate aggregate $[Mn^{III}Mn^{II}L(\mu\text{-}3,5\text{-}DTBC^{2-})]^+$ deserves additional importance because this indicates clear evidence of the coordination and bridging ability of the substrate to the complex catalyst. Moreover, the species mimic the aggregate proposed in one mechanism, at least in terms of stoichiometry (1:1) and coordination mode (bridging).

CONCLUSIONS

Having bis(μ-phenoxo)-μ-carboxylate bridging moiety and also having isolated +III and +II centers, the $Mn^{III}Mn^{II}/Mn^{III}_2Mn^{II}_2$ compounds **1**−**3** represent a new family of valence-trapped dinuclear or dimer-of-dinuclear compounds of manganese. DFT calculated J values properly reproduce the different nature of the $Mn^{III}Mn^{II}$ exchange interactions found in **1**−**3** and also in the only two previously published related compounds. Despite the presence of many structural parameters that can play a significant role in the magnetic properties, the lengths of the Mn^{III}−O distances in the phenoxo exchange pathway involving short Mn^{II}−O distances allow us to explain the changes in the magnetic properties. The relative values of single ion anisotropy of Mn^{III} centers in **1**−**3** could be nicely explained here in terms of direction of the Jahn−Teller axis.

The title compounds are the first examples of dinuclear mixed-valence compounds of manganese showing catechol oxidase activity. The complex−substrate aggregate containing most probably a bridging bidentate catecholate moiety mimic the dicopper(II)−substrate aggregate proposed in one mechanism in terms of stoichiometry (1:1) and coordination mode (bridging).

The synthetic methodology of template condensation of 2,6-diformyl-4-methylphenol and a diamine in presence of manganese(II) perchlorate and sodium carboxylate resulting in the generation of the bis(μ-phenoxo)-μ-carboxylate $Mn^{III}Mn^{II}$ species derived from a symmetric macrocyclic ligand, as described here, can be followed to get similar compounds having variable structural parameters, and the derived mixed-valence systems may be utilized for further exploration of catecholase activity and magnetic properties.

ASSOCIATED CONTENT

Supporting Information

Crystallographic data of **1**−**3** in CIF format, Table S1 with selected structural parameters of **3**, Figures S1−S5 showing spectral profiles of mixtures of the compounds with 3,5-$DTBCH_2$ in MeCN and MeOH, Figures S6−S10 showing rate plots for the catalytic reactions with the compounds, Figures S11 and S12 showing ESI-MS positive spectra for **1** and **3**, respectively, Figure S13 showing $\chi_M T$ vs T plot for **3**, Information about ground state, first excited state, and first excitation energy of complexes **1**−**3**, and Figure S14 showing a scheme of the central core of **3**. These materials are available free of charge via the Internet at http://pubs.acs.org.

AUTHOR INFORMATION

Corresponding Author

*E-mail addresses: sm_cu_chem@yahoo.co.in (S. M.); eliseo.ruiz@qi.ub.es (E. R.).

Notes

The authors declare no competing financial interest.

■ ACKNOWLEDGMENTS

Financial support from Government of India through the Department of Science and Technology (Project No. SR/S1/IC−42/2011) and Council for Scientific and Industrial Research (Fellowship to A. Jana) is gratefully acknowledged. Crystallography was performed at the DST-FIST, India-funded Single Crystal Diffractometer Facility at the Department of Chemistry, University of Calcutta. N.A.-A. and E.R. thank the Ministerio de Educación y Ciencia (Grants CTQ2012-32247/BQU and CTQ2011-23862-C02-01), *Generalitat de Catalunya* (Grant 2009SGR-1459), and ICREA (Institució Catalana de Recerca i Estudis Avançats) for financial support. The authors thankfully acknowledge the computer resources provided by the CESCA.

■ REFERENCES

(1) (a) Robin, M. B.; Day, P. *Adv. Inorg. Chem. Radiochem.* **1967**, *10*, 247. (b) Allen, G. C.; Hush, N. S. *Prog. Inorg. Chem.* **1967**, *8*, 357. (c) Hush, N. S. *Prog. Inorg. Chem.* **1967**, *8*, 391.

(2) (a) Kaim, W.; Lahiri, G. K. *Angew. Chem., Int. Ed.* **2007**, *46*, 1778. (b) Demadis, K. D.; Hartshorn, C. M.; Meyer, T. J. *Chem. Rev.* **2001**, *101*, 2655. (c) Kaim, W.; Klein, A.; Glöckle, M. *Acc. Chem. Res.* **2000**, *33*, 755. (d) D'Alessandro, D. M.; Keene, F. R. *Chem. Rev.* **2006**, *106*, 2270. (e) D'Alessandro, D. M.; Keene, F. R. *Chem. Soc. Rev.* **2006**, *35*, 424. (f) Brunschwig, B. S.; Creutz, C.; Sutin, N. *Chem. Soc. Rev.* **2002**, *31*, 168.

(3) (a) Dutta, S. K.; Ensling, J.; Werner, R.; Flörke, U.; Haase, W.; Gütlich, P.; Nag, K. *Angew. Chem., Int. Ed. Engl.* **1997**, *36*, 152. (b) Drüeke, S.; Chaudhuri, P.; Pohl, K.; Wieghardt, K.; Ding, X.-Q.; Bill, E.; Sawaryn, A.; Trautwein, A. X.; Winkler, H.; Gurman, S. J. *J. Chem. Soc., Chem. Commun.* **1989**, 59.

(4) Hazra, S.; Sasmal, S.; Fleck, M.; Grandjean, F.; Sougrati, M. T.; Ghosh, M.; Harris, T. D.; Bonville, P.; Long, G. J.; Mohanta, S. *J. Chem. Phys.* **2011**, *134*, No. 174507.

(5) (a) Stamatatos, T. C.; Christou, G. *Inorg. Chem.* **2009**, *48*, 3308. (b) Lampropoulos, C.; Redler, G.; Data, S.; Abboud, K. A.; Hill, S.; Christou, G. *Inorg. Chem.* **2010**, *49*, 1325. (c) Taguchi, T.; Wernsdorfer, W.; Abboud, K. A.; Christou, G. *Inorg. Chem.* **2010**, *49*, 10579. (d) Berlinguette, C. P.; Vaughn, D.; Cañada-Vilalta, C.; Galán-Mascarós, J. R.; Dunbar, K. R. *Angew. Chem., Int. Ed.* **2003**, *42*, 1523. (e) Brechin, E. K.; Boskovic, C.; Wernsdorfer, W.; Yoo, J.; Yamaguchi, A.; Sañudo, E. C.; Concolino, T. R.; Rheingold, A. L.; Ishimoto, H.; Hendrickson, D. N.; Christou, G. *J. Am. Chem. Soc.* **2002**, *124*, 9710. (f) Boskovic, C.; Pink, M.; Huffman, J. C.; Hendrickson, D. N.; Christou, G. *J. Am. Chem. Soc.* **2001**, *123*, 9914. (g) Rumberger, E. M.; del Barco, E.; Lawrence, J.; Hill, S.; Kent, A. D.; Zakharov, L. N.; Rheingold, A. L.; Hendrickson, D. N. *Polyhedron* **2005**, *24*, 2557. (h) Ako, A. M.; Hewitt, I. J.; Mereacre, V.; Clérac, R.; Wernsdorfer, W.; Anson, C. E.; Powell, A. K. *Angew. Chem., Int. Ed.* **2006**, *45*, 4926.

(6) (a) Larson, E. J., Pecoraro, V. L., Eds. *Manganese Redox Enzymes*; VCH Publications: New York, 1992; p 1. (b) Crowley, J. D.; Traynor, D. A.; Weatherburn, D. C. *Metal Ions in Biological Processes*; Sigel, A., Sigel, H., Eds.; Marcel, Dekker: Basel, Switzerland, 2000; p 209. (c) Holm, R. H.; Kennepohl, P.; Solomon, E. I. *Chem. Rev.* **1996**, *96*, 2239. (d) Blondin, G.; Girerd, J. J. *Chem. Rev.* **1990**, *90*, 1359.

(7) (a) Mitić, N.; Smith, S. J.; Neves, A.; Guddat, L. W.; Gahan, L. R.; Schenk, G. *Chem. Rev.* **2006**, *106*, 3338. (b) Wilcox, D. E. *Chem. Rev.* **1996**, *96*, 2435.

(8) (a) Yachandra, V. K.; Sauer, K.; Klein, M. P. *Chem. Rev.* **1996**, *96*, 2927. (b) Rutherford, A. W.; Boussac, A. *Science* **2004**, *303*, 1782.

(9) (a) Borgstahl, G. E.; Parge, H. E.; Hickey, M. J.; Johnson, M. J.; Boissinot, M.; Hallewell, R. A.; Lepock, J. R.; Cabelli, D. E.; Tainer, J. A. *Biochemistry* **1996**, *35*, 4287. (b) Whittaker, M. M.; Barynin, V. V.; Antonyuk, S. V.; Whittaker, J. W. *Biochemistry* **1999**, *38*, 9126. (c) Barynin, V. V.; Whittaker, M. M.; Antonyuk, S. V.; Lamzin, V. S.; Harrison, P. M.; Artymiuk, P. J.; Whittaker, J. W. *Structure* **2001**, *9*, 725.

(10) (a) Koval, I. A.; Gamez, P.; Belle, C.; Selmeczi, K.; Reedijk, J. *Chem. Soc. Rev.* **2006**, *35*, 814. (b) Selmeczi, K.; Réglier, M.; Giorgi, M.; Speier, G. *Coord. Chem. Rev.* **2003**, *245*, 191. (c) Than, R.; Feldmann, A. A.; Krebs, B. *Coord. Chem. Rev.* **1999**, *182*, 211.

(11) (a) Solomon, E. I.; Sundaram, U. M.; Machonkin, T. E. *Chem. Rev.* **1996**, *96*, 2563. (b) Kitajima, N.; Moro-oka, Y. *Chem. Rev.* **1994**, *94*, 737. (c) Eicken, C.; Krebs, B.; Sacchettini, J. C. *Curr. Opin. Struct. Biol.* **1999**, *9*, 677.

(12) (a) Majumder, S.; Sarkar, S.; Sasmal, S.; Sañudo, E. C.; Mohanta, S. *Inorg. Chem.* **2011**, *50*, 7540. (b) Belle, C.; Beguin, C.; Gautier-Luneau, I.; Hamman, S.; Philouze, C.; Pierre, J. L.; Thomas, F.; Torelli, S. *Inorg. Chem.* **2002**, *41*, 479. (c) Banerjee, A.; Sarkar, S.; Chopra, D.; Colacio, E.; Rajak, K. K. *Inorg. Chem.* **2008**, *47*, 4023. (d) Kao, C.-H.; Wei, H.-H.; Liu, Y.-H.; Lee, G.-H.; Wang, Y.; Lee, C.-J. *J. Inorg. Biochem.* **2001**, *84*, 171. (e) González-Sebastián, L.; Ugalde-Saldívar, V. M.; Mijangos, E.; Mendoza-Quijano, M. R.; Ortiz-Frade, L.; Gasque, L. *J. Inorg. Biochem.* **2010**, *104*, 1112.

(13) (a) Reim, J.; Krebs, B. *J. Chem. Soc., Dalton Trans.* **1997**, 3793. (b) Anekwea, J.; Hammerschmidta, A.; Rompelb, A.; Krebs, B. *Z. Anorg. Allg. Chem.* **2006**, *632*, 1057. (c) Merkel, M.; Mçller, N.; Piacenza, M.; Grimme, S.; Rompel, A.; Krebs, B. *Chem.−Eur. J.* **2005**, *11*, 1201.

(14) (a) Rey, N. A.; Neves, A.; Bortoluzzi, A. J.; Pich, C. T.; Terenzi, H. *Inorg. Chem.* **2007**, *46*, 348. (b) Ackermann, J.; Meyer, F.; Kaifer, E.; Pritzkow, H. *Chem.−Eur. J.* **2002**, *8*, 247. (c) Mukherjee, J.; Mukherjee, R. *Inorg. Chim. Acta* **2002**, *337*, 429. (d) Fernandes, C.; Neves, A.; Bortoluzzi, J.; Mangrich, A. S.; Rentschler, E.; Szpoganicz, B.; Schwingel, E. *Inorg. Chim. Acta* **2001**, *320*, 12.

(15) (a) Thirumavalavan, M.; Akilan, P.; Kandaswamy, M.; Chinnakali, G.; Senthil Kumar, G.; Fun, H. K. *Inorg. Chem.* **2003**, *42*, 3308. (b) Smith, S. J.; Noble, C. J.; Palmer, R. C.; Hanson, G. R.; Schenk, G.; Gahan, L. R.; Riley, M. *J. Biol. Inorg. Chem.* **2008**, *13*, 499. (c) Manzur, J.; García, A. M.; Vega, A.; Ibañez, A. *Polyhedron* **2007**, *26*, 115. (d) Karlin, K. D.; Gultneh, Y.; Nicholson, T.; Zubieta, J. *Inorg. Chem.* **1985**, *24*, 3725.

(16) (a) Triller, M. U.; Pursche, D.; Hsieh, W.-Y.; Pecoraro, V. L.; Rompel, A.; Krebs, B. *Inorg. Chem.* **2003**, *42*, 6274. (b) Szigyártó, I. C.; Simándi, L. I.; Párkányi, L.; Korecz, L.; Schlosser, G. *Inorg. Chem.* **2006**, *45*, 7480. (c) Kovala-Demertzi, D.; Hadjikakou, S. K.; Demertzis, M. A.; Deligiannakis, Y. *J. Inorg. Biochem.* **1998**, *69*, 223. (d) Gultneh, Y.; Farooq, A.; Karlin, K. D.; Liu, S.; Zubieta, J. *Inorg. Chim. Acta* **1993**, *211*, 171.

(17) (a) Hitomi, Y.; Ando, A.; Matsui, H.; Ito, T.; Tanaka, T.; Ogo, S.; Funabiki, T. *Inorg. Chem.* **2005**, *44*, 3473. (b) Blay, G.; Fernández, I.; Pedro, J. R.; Ruiz-García, R.; Temporal-Sánchez, T.; Pardo, E.; Lloret, F.; Muñoz, M. C. *J. Mol. Catal. A* **2006**, *250*, 20. (c) Kaizer, J.; Csonka, R.; Baráth, G.; Speier, G. *Trans. Metal Chem.* **2007**, *32*, 1047.

(18) Majumder, A.; Goswami, S.; Batten, S. R.; Fallah, M. S. E.; Ribas, J.; Mitra, S. *Inorg. Chim. Acta* **2006**, *359*, 2375.

(19) Mukherjee, S.; Weyhermüller, T.; Bothe, E.; Wieghardt, K.; Chaudhuri, P. *Dalton Trans.* **2004**, 3842.

(20) (a) Simándi, T. L.; Simándi, L. I. *J. Chem. Soc., Dalton Trans.* **1999**, 4529. (b) Simándi, L. I.; Simándi, T. L. *J. Inorg. Biochem.* **2001**, *86*, 332. (c) Simándi, L. I.; Simándi, T. L. *J. Chem. Soc., Dalton Trans.* **1998**, 3275. (d) Rao, C. R. K.; Zacharias, P. S. *Polyhedron* **1997**, *16*, 1201.

(21) Ullman, F.; Brittner, K. *Chem. Ber.* **1909**, *42*, 2539.

(22) (a) *APEX-II*, *SAINT-Plus*, and *TWINABS*, Bruker−Nonius AXS Inc., Madison, Wisconsin, USA, 2004. (b) Sheldrick, G. M. *SAINT* (version 6.02), *SADABS* (version 2.03), Bruker AXS Inc., Madison, WI, 2002. (c) Sheldrick, G. M. *SHELXTL* (version 6.10), Bruker AXS Inc., Madison, WI, 2002. (d) Sheldrick, G. M. *SHELXL-97*, Crystal Structure Refinement Program, University of Göttingen, Germany, 1997.

(23) (a) Ruiz, E.; Alemany, P.; Alvarez, S.; Cano, J. *J. Am. Chem. Soc.* **1997**, *119*, 1297. (b) Ruiz, E.; Cano, J.; Alvarez, S. *Chem.−Eur. J.* **2005**,

11, 4767. (c) Ruiz, E.; Cauchy, T.; Cano, J.; Costa, R.; Tercero, J.; Alvarez, S. *J. Am. Chem. Soc.* **2008**, *130*, 7420.
(24) (a) Ruiz, E. *Struct. Bonding (Berlin)* **2004**, *113*, 71. (b) Ruiz, E.; Alvarez, S.; Cano, J.; Polo, V. *J. Chem. Phys.* **2005**, *123*, No. 164110(1).
(25) Ruiz, E.; Cano, J.; Alvarez, S.; Alemany, P. *J. Comput. Chem.* **1999**, *20*, 1391.
(26) Ruiz, E.; Rodríguez-Fortea, A.; Cano, J.; Alvarez, S.; Alemany, P. *J. Comput. Chem.* **2003**, *24*, 982.
(27) Ruiz, E.; Rodríguez-Fortea, A.; Tercero, J.; Cauchy, T.; Massobrio, C. *J. Chem. Phys.* **2005**, *123*, No. 074102(1).
(28) Becke, A. D. *J. Chem. Phys.* **1993**, *98*, 5648.
(29) Schaefer, A.; Huber, C.; Ahlrichs, R. *J. Chem. Phys.* **1994**, *100*, 5829.
(30) Frisch, M. J.; Trucks, G. W.; Schlegel, H. B.; Scuseria, G. E.; Robb, M. A.; Cheeseman, J. R.; Scalmani, G.; Barone, V.; Mennucci, B.; Petersson, G. A.; Nakatsuji, H.; Caricato, M.; Li, X.; Hratchian, H. P.; Izmaylov, A. F.; Bloino, J.; Zheng, G.; Sonnenberg, J. L.; Hada, M.; Ehara, M.; Toyota, K.; Fukuda, R.; Hasegawa, J.; Ishida, M.; Nakajima, T.; Honda, Y.; Kitao, O.; Nakai, H.; Vreven, T.; Montgomery, J. A., Jr.; Peralta, J. E.; Ogliaro, F.; Bearpark, M.; Heyd, J. J.; Brothers, E.; Kudin, K. N.; Staroverov, V. N.; Kobayashi, R.; Normand, J.; Raghavachari, K.; Rendell, A.; Burant, J. C.; Iyengar, S. S.; Tomasi, J.; Cossi, M.; Rega, N.; Millam, J. M.; Klene, M.; Knox, J. E.; Cross, J. B.; Bakken, V.; Adamo, C.; Jaramillo, J.; Gomperts, R.; Stratmann, R. E.; Yazyev, O.; Austin, A. J.; Cammi, R.; Pomelli, C.; Ochterski, J. W.; Martin, R. L.; Morokuma, K.; Zakrzewski, V. G.; Voth, G. A.; Salvador, P.; Dannenberg, J. J.; Dapprich, S.; Daniels, A. D.; Farkas, O.; Foresman, J. B.; Ortiz, J. V.; Cioslowski, J.; Fox, D. J. *Gaussian 09*, revision A.1; Gaussian, Inc.: Wallingford, CT, 2009.
(31) *Jaguar 7.0*, Schrödinger, LLC, New York, 2007.
(32) Vacek, G.; Perry, J. K.; Langlois, J.-M. *Chem. Phys. Lett.* **1999**, *310*, 189.
(33) (a) Nakamoto, K. *Infrared and Raman Spectra of Inorganic and CoordinationCompounds*, 3rd ed.; John Wiley: New York, 1978; p 232. (b) Socrates, G. *Infrared Characteristic Group Frequencies: Tables and Charts*, 3rd ed.; Wiley: Chichester, U.K., 2001.
(34) Geary, W. J. *Chem. Rev.* **1971**, *7*, 81.
(35) Liu, W.; Thorp, H. H. *Inorg. Chem.* **1993**, *32*, 4102.
(36) (a) Wilkins, R. G. *Kinetics and Mechanism of Reactions of Transition Metal Complexes*; Wiley-VCH Verlag GmbH & Co. KGaA: Weinheim, Germany, 2002; p 4. (b) Volkmer, D.; Hommerich, B.; Griesar, K.; Haase, W.; Krebs, B. *Inorg. Chem.* **1996**, *35*, 3792.
(37) (a) Borrás-Almenar, J. J.; Clemente-Juan, J. M.; Coronado, E.; Tsukerblat, B. S. *Inorg. Chem.* **1999**, *38*, 6081. (b) Borrás-Almenar, J. J.; Clemente, J. M.; Coronado, E.; Tsukerblat, B. S. *J. Comput. Chem.* **2001**, *22*, 985.
(38) (a) Mennedy, B. J.; Murray, K. S. *Inorg. Chem.* **1985**, *24*, 1552. (b) Taking into account that **1** and **2** could be seen as mononuclear species with intermolecular interactions.
(39) (a) Gerritsen, H. J.; Sabinsky, E. S. *Phys. Rev.* **1963**, *132*, 1507. (b) Miyasaka, H.; Saitoh, A.; Abe, S. *Coord. Chem. Rev.* **2007**, *251*, 2622.
(40) (a) Ruiz, E.; Cuachy, T.; Cano, J.; Costa, R.; Tercero, J.; Alvarez, S. *J. Am. Chem. Soc.* **2008**, *130*, 7420. (b) Rich, J.; Castillo, C. E.; Romero, I.; Rodríguez, M.; Duboc, C.; Collomb, M.-N. *Eur. J. Inorg. Chem.* **2010**, 3658. (c) Dubo, C.; Collomb, M.-N.; Neese, R. *Appl. Magn. Reson.* **2010**, *37*, 229.
(41) (a) Chang, H.-R.; Larsen, S. C.; Boyd, P. D. W.; Pierpont, C. G.; Hendrickson, D. N. *J. Am. Chem. Soc.* **1988**, *110*, 4565. (b) Gou, S.; Zeng, Q.; Yu, Z.; Qian, M.; Zhu, J.; Duan, C.; You, X. *Inorg. Chim. Acta* **2000**, *303*, 175.
(42) (a) Liu, H.; Tian, J.; Kou, Y.; Zhang, H.; Feng, L.; Li, D.; Gu, W.; Liu, X.; Liao, D.; Cheng, P.; Ribas, J.; Yan, S. *Dalton Trans.* **2009**, 10511. (b) Gultneh, Y.; Tesema, Y. T.; Yisgedu, T. B.; Butcher, R. J.; Wang, G.; Yee, G. T. *Inorg. Chem.* **2006**, *45*, 3023. (c) Schake, A. R.; Schmitt, E. A.; Conti, A. J.; Streib, W. E.; Huffman, J. C.; Hendrickson, D. N.; Christou, G. *Inorg. Chem.* **1991**, *30*, 3192. (d) Diril, H.; Chang, H.-R.; Nilges, M. J.; Zhang, X.; Potenza, J. A.; Schugar, H. J.; Isied, S. S.; Hendrickson, D. N. *J. Am. Chem. Soc.* **1989**, *111*, 5102. (e) Buchanan, R. M.; Oberhausen, K. J.; Richardson, J. F. *Inorg. Chem.* **1988**, *27*, 971.
(43) (a) Dubois, L.; Xiang, D.-F.; Tan, X.-H.; Pécaut, J.; Jones, P.; Baudron, S.; Pape, L. L.; Latour, J.-M.; Baffert, C.; Chardon-Noblat, S.; Collomb, M.-N.; Deronzier, A. *Inorg. Chem.* **2003**, *42*, 750. (b) Smith, S. J.; Riley, M. J.; Noble, C. J.; Hanson, G. R.; Stranger, R.; Jayaratne, V.; Cavigliasso, G.; Schenk, G.; Gahan, L. R. *Inorg. Chem.* **2009**, *48*, 10036.
(44) (a) Goodenough, J. B. *Phys. Rev.* **1955**, *100*, 564. (b) Kanamori, J. *J. Phys. Chem. Solids* **1959**, *10*, 87.
(45) (a) Rodríguez-Fortea, A.; Alemany, P.; Alvarez, S.; Ruiz, E. *Chem.—Eur. J.* **2001**, *7*, 627. (b) Colacio, E.; Domínguez-Vera, J.; Ghazi, M.; Kivekäs, R.; Klinga, M.; Moreno, J. M. *Eur. J. Inorg. Chem.* **1999**, 441.
(46) Cano, J.; Ruiz, E.; Alvarez, S.; Verdaguer, M. *Comments Inorg. Chem.* **1998**, *20*, 27.
(47) Ruiz, E.; Cirera, J.; Alvarez, S. *Coord. Chem. Rev.* **2005**, *249*, 2649.
(48) Awaga, K.; Suzuki, Y.; Hachisuka, H.; Takeda, K. *J. Mater. Chem.* **2006**, *16*, 2516.